

5. Drag: An Introduction

5.1 The Importance of Drag

The subject of drag didn't arise in our use of panel methods to examine the inviscid flowfield around *airfoils* in the last chapter: the theoretical drag was always zero! Before proceeding further in any study of computational aerodynamics the issue of drag must be addressed. There are many sources of drag. In three-dimensional flow, and in two dimensions when compressibility becomes important, drag occurs even when the flow is assumed inviscid. Before discussing the aerodynamics of lifting systems, the fundamental aspects of aerodynamic drag will be examined.

Drag is at the heart of aerodynamic design. The subject is fascinatingly complex. All aerodynamicists secretly hope for negative drag. The subject is tricky and continues to be controversial. It's also terribly important. Even seemingly minor changes in drag can be critical. On the Concorde, a one count drag increase ($\Delta C_D = .0001$) requires two passengers, out of the 90 ~ 100 passenger capacity, be taken off the North Atlantic run.¹ In design studies a drag decrease is equated to the decrease in aircraft weight required to carry a specified payload the required distance. One advanced fighter study² found the drag sensitivity in supersonic cruise was 90 lb/ct and 48 lb/ct for subsonic/transonic cruise. At the transonic maneuver design point the sensitivity was 16 lb/ct (drag is very high here). In comparison, the growth factor was 4.1 lb of takeoff gross weight for

every 1 lb of fixed weight added. For one executive business jet the range sensitivity is 17 miles/drag count. Advanced supersonic transports now being studied have range sensitivities of about 100 miles/drag count. When new aircraft are sold, the sales contract stipulates numerous performance guarantees. One of the most important is range. The aircraft company guarantees a specified range before the aircraft is built and tested. The penalty for failure to meet the range guarantee is severe. Conservative drag projections aren't allowed—the competition is so intense that in the design stage the aerodynamicist will be pressured to make optimistic estimates. In one briefing in the early '80s, an aerodynamicist for a major airframer said that his company was willing to invest \$750,000 for each count of drag reduction. Under these conditions the importance of designing for low drag, and the ability to estimate drag, can hardly be overstated.

The economic viability and future survival of an aircraft manufacturer depends on minimizing aerodynamic drag (together with the other design key technologies of structures, propulsion, and control) while maintaining good handling qualities to ensure flight safety and ride comfort. New designs that employ advanced computational aerodynamics methods are needed to achieve vehicles with less drag than current aircraft. The most recent generation of designs (Boeing 767, 777, Airbus A340, *etc.*) already take advantage of computational aerodynamics, advanced experimental methods, and years of experience. Future advances in aerodynamic performance present tough challenges requiring both innovative concepts and the very best methodology possible.

Initial drag estimates can dictate the selection of a specific configuration concept in comparison with other concepts early in the design phase. The drag projections have a huge effect on the projected configuration size and cost, and thus on the decision to proceed with the design.

There are two other key considerations in discussing drag. First, drag cannot yet be predicted accurately with high confidence levels³ (especially for unusual configuration concepts) without extensive testing, and secondly, no one is exactly sure what the ultimate possible drag level really is that can be achieved for a practical configuration. To this extent, aerodynamic designers are the dreamers of the engineering profession.

Because of its importance, AGARD has held numerous conferences devoted to drag and its reduction. In addition to the study of computational capability cited above, AGARD publications include CP-124,⁴ CP-264,⁵ R-723⁶ and R-786⁷. These reports provide a wealth of information.

An AIAA Progress Series book has also been devoted primarily to drag.⁸ Chapters discuss the history of drag prediction, typical methods currently used to predict drag, and the intricacies of drag prediction for complete configurations. The most complete compilation of drag information available is due to Hoerner.⁹ In this chapter we introduce the key concepts required to use computational aerodynamics to evaluate drag. Additional discussion is included in the chapters on viscous effects, transonic, and supersonic aerodynamics.

5.2 Some Different Ways to View Drag - Nomenclature and Concepts

In discussing drag, the numerous viewpoints that people use to think about drag can create confusion. Here we illustrate the problem by defining drag from several viewpoints. This provides an opportunity to discuss various basic drag concepts.

1. *Simple Integration*: Consider the distribution of forces over the surface. This includes a pressure force and a shear stress force due to the presence of viscosity. This approach is known as a nearfield drag calculation. An accurate integration will result in an accurate estimate of the drag. However, two problems exist:

- i) This integration requires extreme precision (remember that program PANEL did not predict exactly zero drag).
- ii) The results are difficult to interpret for aerodynamic analysis. Exactly where is the drag coming from? Why does it exist, and how do you reduce it?

Thus in most cases a simple integration over the surface is not satisfactory for use in aerodynamic design. Codes have only recently begun to be fairly reliable for nearfield drag estimation, and then only for certain specific types of problems. The best success has been achieved for airfoils, and even there the situation still isn't perfect (see Chapters 10 and 11).

2. *Fluid Mechanics*: This viewpoint emphasizes the drag resulting from various fluid mechanics phenomena. This approach is important in conceiving a means to reduce drag. It also provides a means of computing drag contributions in a systematic manner. Thinking in terms of components from different physical effects, a typical drag breakdown would be:

- friction drag
- form drag
- induced drag
- wave drag.

Each of these terms will be defined below. Figure 5-1 illustrates possible ways to find the total drag. It is based on a figure in Torenbeek's book.¹⁰ He also has a good discussion of drag and its estimation. Clearly, the subject can be confusing.

3. *Aerodynamics*: This approach combines the fluid mechanics viewpoint with more practical considerations. From the aerodynamic design aspect it proves useful to think in terms of contributions from a variety of aircraft features. This includes effects due to the requirement to trim the aircraft, and interactions between the aerodynamics of the vehicle and both propulsion induced flow effects and structural deformation effects. Within this context, several other considerations are identified. The basic contributions from each component must be included. This leads to a drag analysis based on typical configuration features, as shown below:

- individual component contributions to drag
- base drag
- inlet drag with spillage
- boattail drag
- camber drag
- trim drag
- thrust-drag bookkeeping
- aeroelastic effects on drag

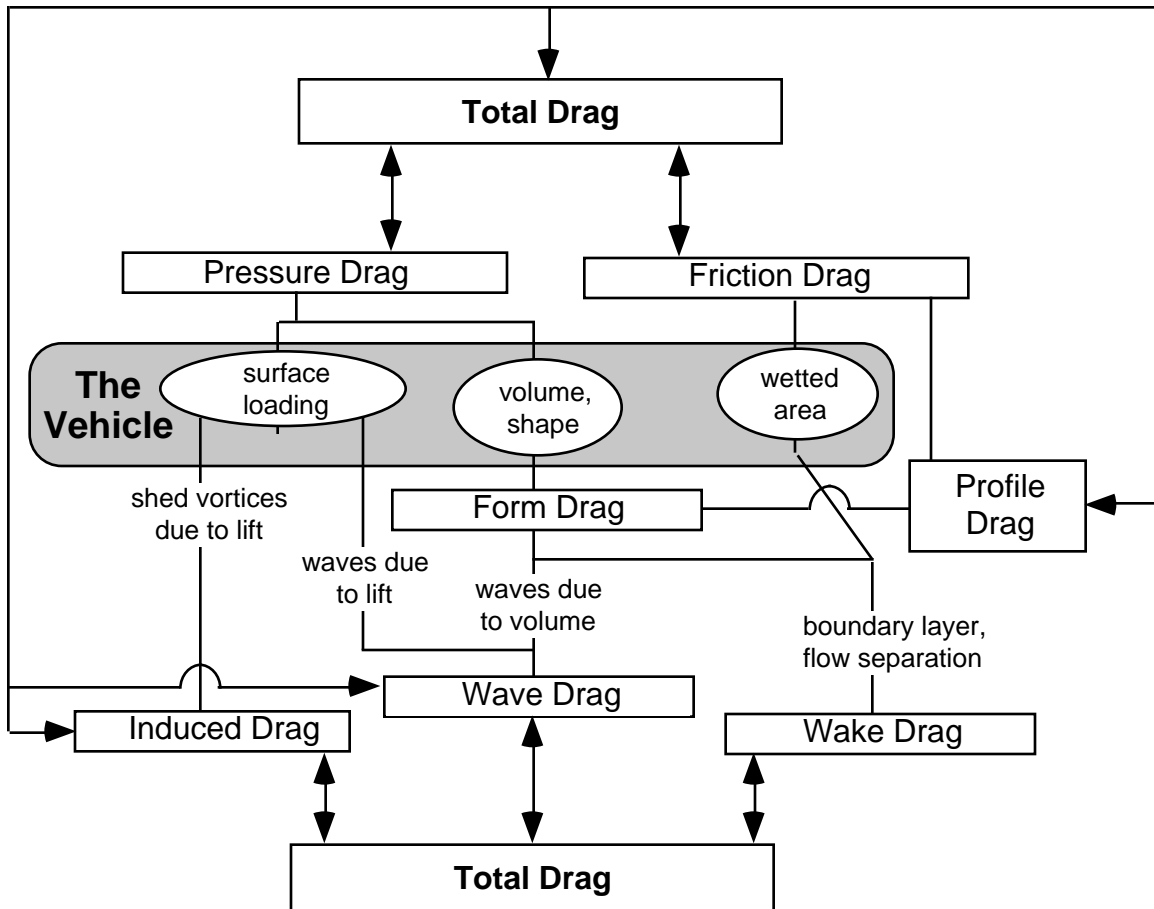


Fig. 5-1. Drag breakdown possibilities (internal flow neglected).

4. *Performance:* To calculate the performance of an airplane it is natural to define drag as the sum of the drag at zero lift and the drag due to lift. This is the approach that leads to the typical drag polar equation:

$$C_D = C_{D_0} + \frac{C_L^2}{\pi A R E} \quad (5-1)$$

Here each term is a function of Mach number, Reynolds number (in practice this is given to the performance group in terms of Mach number and altitude), and the particular geometric configu-

ration (flap deflection, wing sweep, *etc.*). The drag is not precisely a quadratic function of the lift, and the value of the Oswald efficiency factor, E , in Eq.(5-1) is defined as a function of the lift coefficient and Mach number: $E = E(C_L, M)$. The drag also depends on the throttle setting, but that effect is usually included in the thrust table, as discussed below. There is another drag polar approximation that is seen often. This approximation is more commonly used by aerodynamic designers trying to understand wing performance. It is used to take into account the effect of wing camber and twist, which causes the drag polar to be displaced “upward”, becoming asymmetrical about the $C_L = 0$ axis. It is given as:

$$C_D = C_{D_0} + \Delta C_{D_m} + K(C_L - C_{L_m})^2 \quad (5-2)$$

In taking into account the effect of camber and twist on shifting the polar, the ΔC_{D_m} term represents a penalty associated with using twist and camber to achieve good performance at the design lift coefficient. This equation is for a fixed geometry. Figure 5-2 shows how this looks (ΔC_{D_m} is exaggerated for emphasis). The value of K defines the shape of the polar. C_{D_0} represents the minimum drag of the configuration without camber and twist. The values of ΔC_{D_m} and C_{L_m} are functions of the design lift coefficient. Sometimes novice aerodynamicists fail to include ΔC_{D_m} properly and obtain incorrect values of E when evaluating published drag polars. This type of polar shape will be discussed in more detail later in this chapter. Advanced design concepts such as the X-29 minimize this penalty by defining a device schedule to maximize performance across a broad range of lift coefficients.

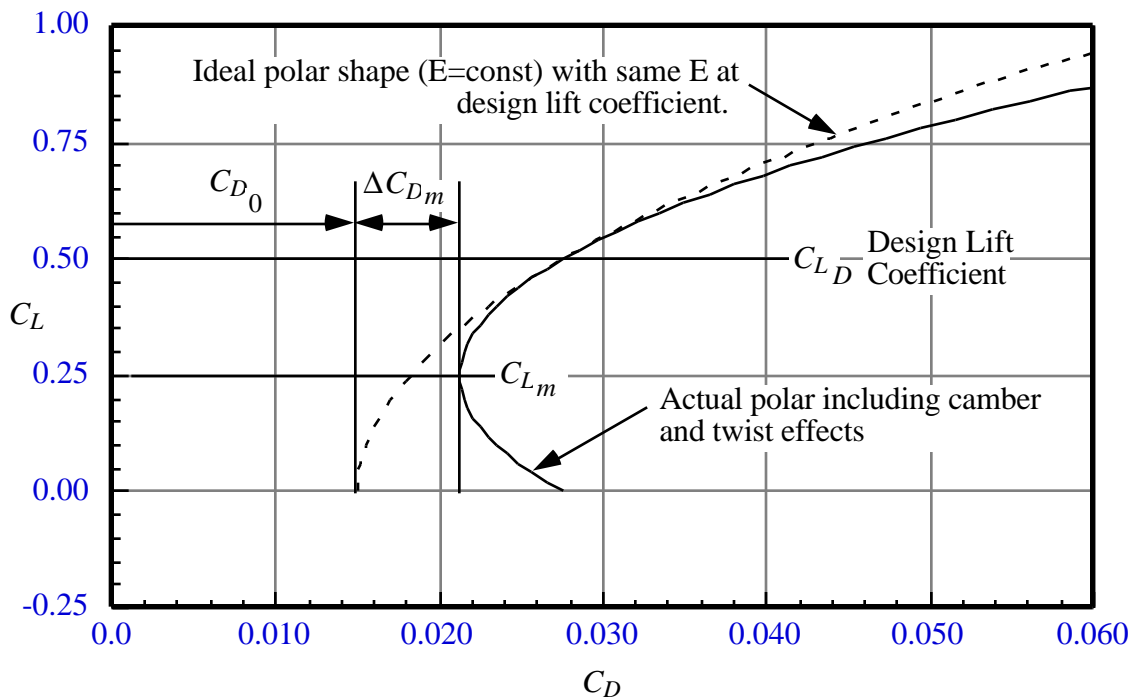


Figure 5-2. Drag polar

As mentioned above, basic drag nomenclature is frequently more confused than it needs to be, and sometimes the nomenclature gets in the way of technical discussions. The chart in Fig. 5-3 provides a basic classification of drag for overview purposes. The aerodynamic configuration-specific approach to drag is not covered in fluid mechanics oriented aerodynamics texts, but is described in aircraft design books. Two other good references are the recent books by Whitford¹¹ and Huenecke.¹² An approach to the evaluation of drag performance, including the efficiency achieved on actual aircraft, was presented by Haines.¹³

We need to define several of these concepts in more detail. The most important overview of aerodynamic drag for design has been given by Küchemann,¹⁴ and should be studied for a complete understanding of drag concepts.

A fluid mechanics refinement: transonic wave drag.

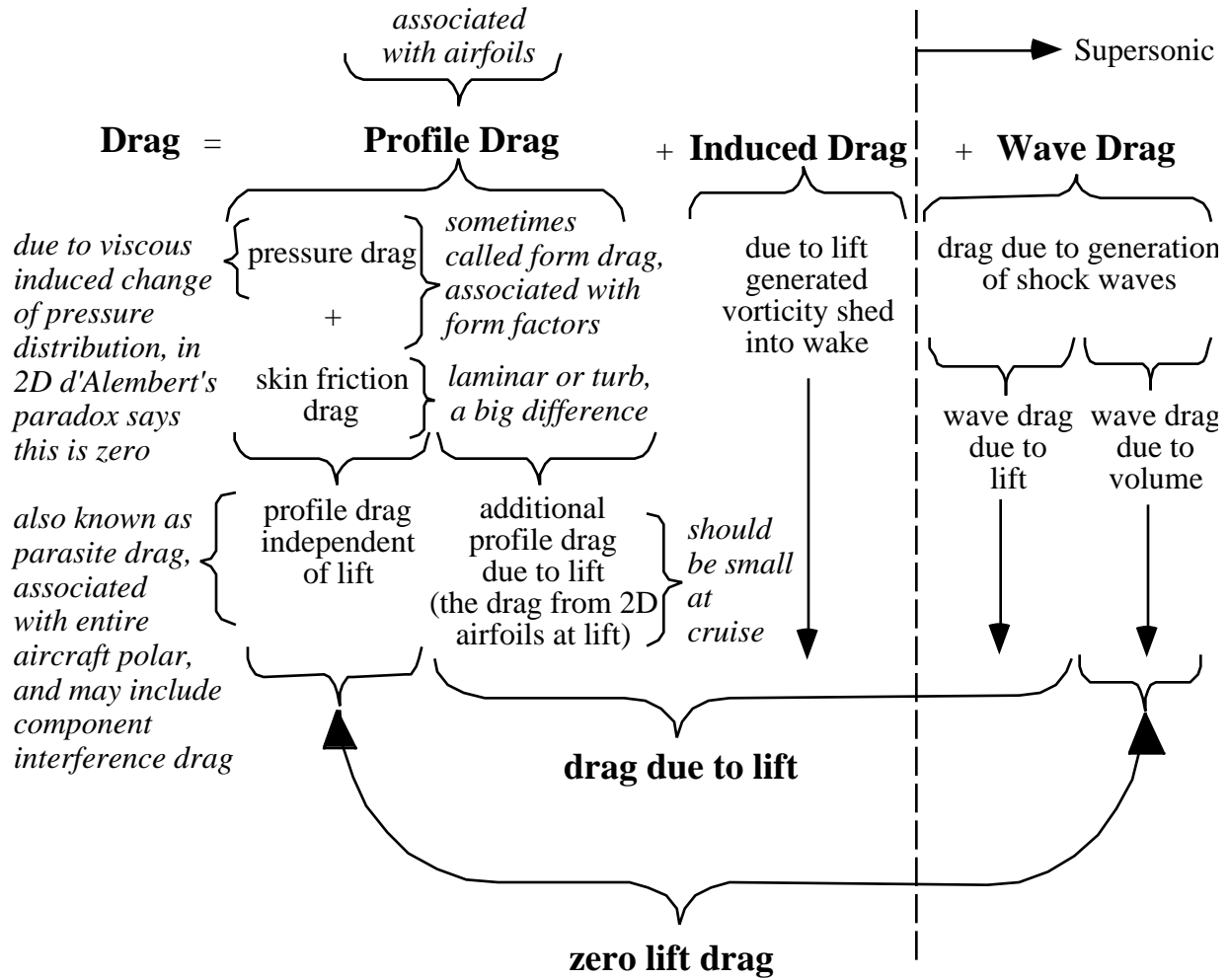
The broadbrush picture of drag presented in Fig. 5.3 suggests that wave drag appears suddenly at supersonic speeds. A more refined examination shows that wave drag arises at subsonic speeds when the flow accelerates locally to supersonic speeds, and then returns to subsonic speed through a shock wave. This leads to the presence of wave drag at subsonic (actually, by definition, transonic) freestream speeds. This initial drag increase, known as *drag rise*, is followed by a rapid increase in drag, and is an important consideration in the design of wings and airfoils. The Mach number at which the rapid drag increase occurs is known as the *drag divergence Mach number*, M_{DD} . The increase in drag occurs directly because of the wave drag associated with the presence of shock waves. However, the drag also increases because the boundary layer thickness increases due to the sudden pressure rise on the surface due to the shock wave, which leads to increased profile drag. Lynch¹⁵ has estimated that at drag divergence the additional transonic drag is approximately evenly divided between the explicit shock drag and the shock induced additional profile drag. Several definitions of the drag rise Mach number are commonly used. The specific definition is usually not important because at drag divergence the drag rises very rapidly and the definitions all result in similar values of M_{DD} .

One standard definition of M_{DD} is the Mach number where

$$\left. \frac{dC_D}{dM} \right|_{C_L=const.} = 0.1. \quad (5-3)$$

Another definition of drag rise is the Mach number at which

$$\Delta C_D = .0020 \text{ from the subsonic value.} \quad (5-4)$$



Note: A straight surface pressure integration makes it very difficult to separate contributors to the total drag - and this is important in aerodynamic design.

Figure 5-3. A Broadbrush categorization of drag.

Commercial transports fly at or close to M_{DD} , and the drag divergence Mach number is a key part of the performance guarantee. Figure 5.4 (data from Shevell¹⁶) illustrates this refinement to Fig. 5-3, together with the definitions associated with the drag rise. The figure also illustrates a common characteristic, “drag creep,” which occurs with many transonic designs.

An aerodynamics/flight mechanics refinement: trim drag.

A drag not directly related directly to pure fluid mechanics arises from the need to trim the vehicle ($C_m = 0$ about the center of gravity) for steady flight. This requirement can lead to control surface deflections that increase (or decrease) the drag. It can be especially important for supersonic aircraft because of the shift in the aerodynamic center location with Mach number. Other cases with significant trim drag may include configurations with variable wing sweep and the use of airfoils with large values of the zero lift pitching moment about their aerodynamic center. Trim drag details are presented in Section 5.10.

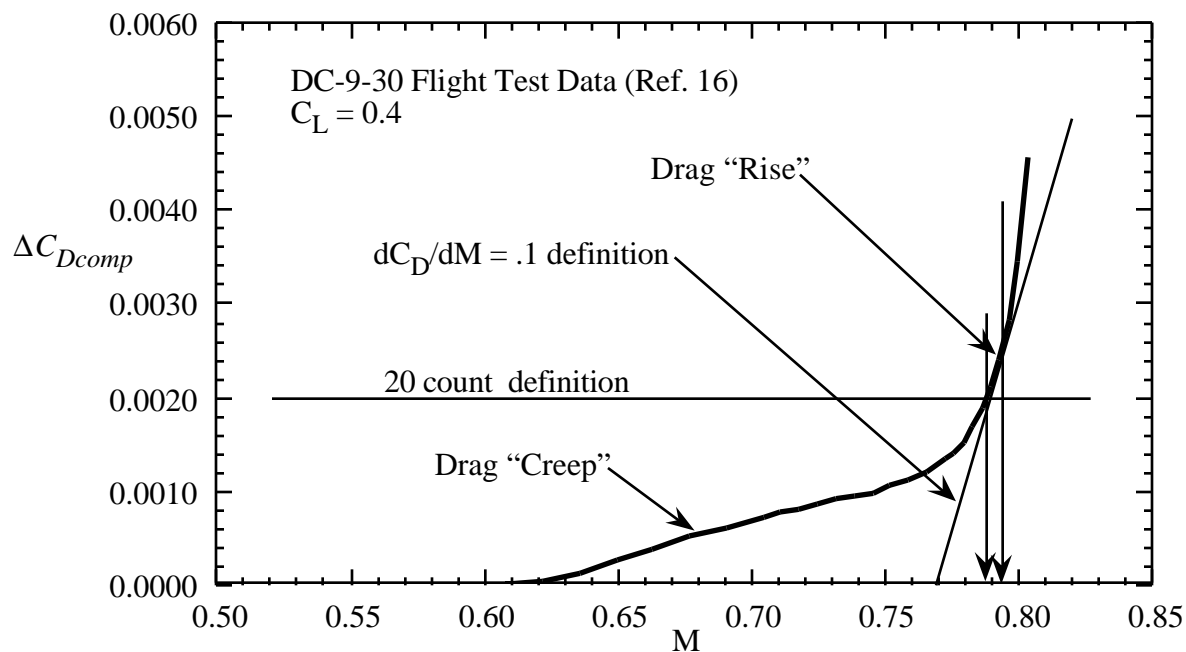


Figure 5.4 Details of wave drag increases at transonic speeds.

A practical aspect of aero-propulsion integration: thrust-drag bookkeeping

To determine aircraft performance, the key value is actually not drag, but the balance between thrust and drag. The drag of the airframe is affected by the operation of the propulsion system, and care must be taken to understand and define these interactions. The amount of air used by the engine defines the size of the streamtube entering the inlet. If all the air in front of the inlet does not enter the inlet, a *spillage drag* will result. Similarly, the boattail drag over the external portion of the nozzle will depend on the nozzle setting in the case of engines with afterburners, and the pressure of the nozzle flow. The definition of a system to properly account for aero-propulsion interactions on the specification of thrust minus drag values is known as thrust-drag bookkeeping. Since thrust is usually provided by the propulsion group, and drag is provided by the aerodynamics group, significant errors in the estimation of aircraft performance have occurred when the necessary coordination and adjustments were not made. The details of this procedure are described in the article by Rooney.¹⁷

Generally, the aerodynamics group provides the performance group with a reference drag polar, and all thrust dependent corrections to the drag polar are accounted for by making adjustments to the thrust values. This is done because it is natural to establish a performance calculation procedure using this approach. The precise details are not important as long as everyone involved in the performance prediction agrees to a specific approach. Usually this requires a specific document defining thrust-drag bookkeeping for each aircraft project.

Aerodynamic-structural interaction: aeroelastic effects on drag

This issue is not strictly a drag consideration, but can make a contribution to the drag if it is not addressed. Aircraft structures deform due to air loads. If the design is centered around a single design point, the aerodynamic shape at the design point can be defined, and the structural analysts will adjust for structural deformation, specifying a “jig shape” that will produce the desired aerodynamic shape at the design point. This is harder to do if there are multiple design points. Deformation of wind tunnel models should also be considered when estimating drag.

5.3 Farfield Drag Analysis

We can estimate the drag on a body most accurately when our predictions methods are not exact by considering the overall momentum balance on a control volume surface well away from the body—a farfield calculation. This is much less sensitive to the detailed calculations of surface pressure and integration of the pressures over the surface to obtain the drag.

The farfield analysis makes use of the momentum theorem. References containing good derivations are by Ashley and Landahl,¹⁸ sections 1.6, 6.6, 7.3 and 9.2, and Heaslet and Lomax,¹⁹ pages 221-229.

For a surface S , which encloses the volume containing an aerodynamic body, the force can be determined by balancing the momentum across S :

$$\mathbf{F} = -\iint_S (p - p_\infty) d\mathbf{S} - \iint_S \rho \mathbf{q} [(\mathbf{V}_\infty + \mathbf{q}) \cdot d\mathbf{S}] \quad (5-5)$$

where \mathbf{q} is the disturbance velocity vector,

$$\mathbf{V} = \mathbf{V}_\infty + \mathbf{q} . \quad (5-6)$$

Define a control volume for use in Eq.(5-5) as shown in Fig. 5-5.

Consider flows far enough away from the body such that linearized flow relations are valid; and use the small disturbance relations:

$$\rho \cong \rho_\infty \left(1 - M_\infty \frac{u}{U_\infty} \right) \quad (5-7)$$

and

$$(p - p_\infty) \cong -\left[U_\infty u + \frac{1}{2}(u^2 + v^2 + w^2) \right] + \frac{1}{2} \rho_\infty M_\infty^2 u^2 . \quad (5-8)$$

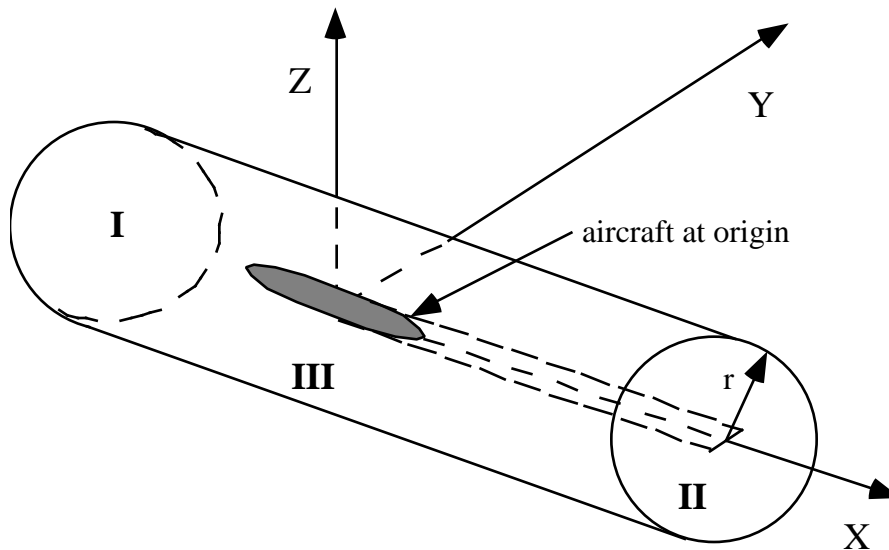


Figure 5-5. Control volume for farfield drag evaluation.

Now, consider the drag component of Eq. (5-5), making use of Eq. (5-7) and Eq. (5-8):

$$D = \frac{1}{2} \rho_{\infty} \iint_{I+II} [(M_{\infty}^2 - 1)u^2 + v^2 + w^2] dydz - \rho_{\infty} \iint_{III} uv_r r d\theta dx \quad (5-9)$$

and v_r is the radial component, $v_r^2 = v^2 + w^2$, where $r^2 = x^2 + y^2$.

Considering the control volume shown in Fig. 5-5, place **I** and **II** far upstream and downstream and make r large. Then, the integral over **I** is zero as $x \rightarrow -\infty$. The integral over **II** as $x \rightarrow \infty$, corresponds to the so-called Trefftz Plane. The integral over **III** is the wave drag integral, which is zero for subsonic flow, and when any embedded shock waves do not reach **III**.

*Consider the integral over **III***

This is the farfield wave drag integral. This integral corresponds to the last term on the right hand side of Eq. (5-9), and can be written as:

$$D_w = \lim_{r \rightarrow \infty} \left(-\rho_{\infty} r \int_0^{2\pi} d\theta \int_{-\infty}^{+\infty} uv_r dx \right) \quad (5-10)$$

If $u, v_r \rightarrow 0$ as $r \rightarrow \infty$ then $D_w = 0$. Thus, when the flow is subsonic there is no wave drag, as we already know. However, if the flow is supersonic, and shock waves are generated, the inte-

gral is not zero. This integral can be calculated for any numerical solution. In this analysis we assume that the flow is governed by the Prandtl-Glauert equation:

$$(1 - M_\infty^2)\phi_{xx} + \phi_{yy} + \phi_{zz} = 0, \tag{5-11}$$

which implies small disturbance flow. This is valid if the vehicle is highly streamlined, as any supersonic vehicle must be. However, since far from the disturbance this equation will model flows from any vehicle, this is not a significant restriction.

To obtain an expression for ϕ that can be used to calculate the farfield integral, assume that the body can be represented by a distribution of sources on the x -axis (the aircraft looks very “slender” from far away). To illustrate the analysis, assume that the body is axisymmetric. Recall that there are different forms for the subsonic and supersonic source:

$$\begin{aligned} \phi &= -\frac{1}{4\pi} \frac{1}{\sqrt{x^2 + \beta^2 r^2}}, & \phi &= -\frac{1}{2\pi} \frac{1}{\sqrt{x^2 - \beta^2 r^2}} \\ &\text{subsonic source} & &\text{supersonic source} \\ &\downarrow & &\downarrow \\ &\phi \rightarrow 0 \text{ as } r \rightarrow \infty & &\phi \rightarrow 0 \text{ as } r \rightarrow \infty \text{ except} \\ & & &\text{as } r \rightarrow \frac{x}{\beta} \end{aligned} \tag{5-12}$$

This means that the integral will have a contribution along the Mach wave independent of how far away the outer control volume is taken. Figure 5-6 illustrates this effect. The resulting force is exactly what is expected—the shock wave contribution to drag: the wave drag.

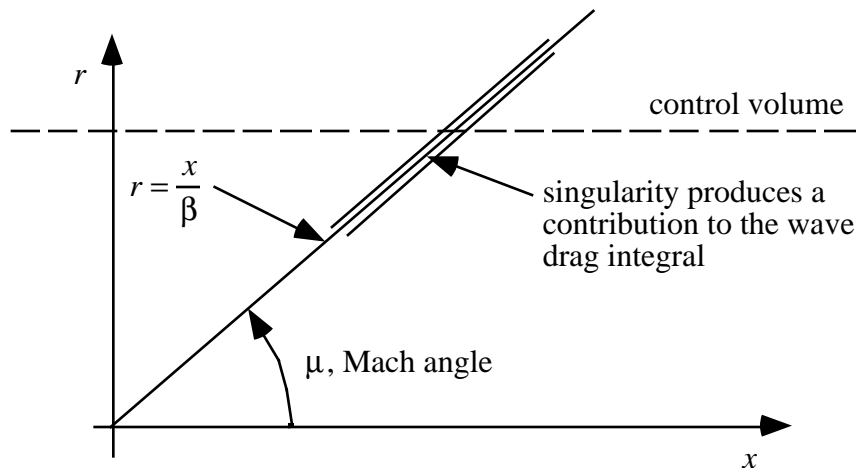


Figure 5-6. Behavior of disturbances along Mach lines in the farfield.

The farfield behavior of the source singularity given in Eq.(5-12) can be used to obtain an expression for the farfield integral in terms of geometric properties of the aircraft. A complete analysis is given in Ashley and Landahl,¹⁸ and Liepman and Roshko.²⁰ The key connection is the assumption relating the supersonic source strength and aircraft geometry. The approximate boundary conditions on the surface equate the change of cross-sectional area to the supersonic source strength: $\sigma(x) = S'(x)$. One required assumption is that the cross-sectional area distribution, $S(x)$, satisfies $S'(0) = S'(l) = 0$. After some algebra the desired relation is obtained:

$$\bar{D}(\theta)_w = -\frac{\rho_\infty U_\infty^2}{4\pi} \int_0^l \int_0^l S''(x_1)S''(x_2) \ln|x_1 - x_2| dx_1 dx_2 . \quad (5-13)$$

This is the wave drag integral. The standard method for evaluation of this integral is available in a program known as the ‘‘Harris Wave Drag’’ program.²¹ That program determines the cross-sectional area distribution of the aircraft and then evaluates the integral numerically. Note that as given above, the Mach number doesn’t appear explicitly. A refined analysis¹⁸ for bodies that aren’t extremely slender extends this approach by taking slices, or *Mach cuts*, of the area through the body at the Mach angle. This is how the Mach number dependence enters the analysis. Finally, for non-axisymmetric bodies the area associated with the Mach cuts changes for each angle around the circumferential integral for the cylindrical integration over Region **III** in Fig. 5-5. Thus the area distribution must be computed for each angle. The total wave drag is then found from

$$D_w = \frac{1}{2\pi} \int_0^{2\pi} \bar{D}_w(\theta) d\theta . \quad (5-14)$$

Examples of the results obtained using this computational method are given in Section 5.7, a discussion of the area rule.

*Consider the integral over **II***

This is the first integral in Eq. (5-9), the induced drag integral:

$$D_i = \frac{1}{2} \rho_\infty \int_{-\infty}^{\infty} \int_{-\infty}^{\infty} \left[(M_\infty^2 - 1)u^2 + v^2 + w^2 \right] dy dz, \quad (5-15)$$

Note that many supersonic aerodynamicists call this the vortex drag, D_v , since it is associated with the trailing vortex system. However, it is in fact the induced drag. The term vortex drag is

confusing in view of the current use of the term “vortex” to denote effects associated with other vortex flow effects (described in Chapter 6). Far downstream, $u \rightarrow 0$, and we are left with the v and w components of velocity induced by the trailing vortex system. The trailing vortex sheet can be thought of as legs of a horseshoe vortex. Thus the integral becomes:

$$D_t = \frac{1}{2} \rho_\infty \int_{-\infty}^{\infty} \int_{-\infty}^{\infty} (v^2 + w^2) dy dz, \quad (5-16)$$

which relates the drag to the kinetic energy of the trailing vortex system.

Now, the flow is governed downstream by the Prandtl-Glauert equation (even if the flow at the vehicle has large disturbances, the perturbations decay downstream):

$$(1 - M_\infty^2) \phi_{xx} + \phi_{yy} + \phi_{zz} = 0 \quad (5-11)$$

and as $x \rightarrow \infty$, $u = 0$, and $u_x = \phi_{xx} = 0$. As a result, the governing equation for the disturbance velocities is Laplace’s Equation for the crossflow velocity:

$$\phi_{yy} + \phi_{zz} = 0. \quad (5-17)$$

An interesting result arises here. The induced drag is explicitly independent of Mach number effects. The analysis is valid for subsonic, transonic and supersonic flows. The Mach number only enters the problem in an indirect manner through the boundary conditions, as we will see.

We now use Green’s Theorem, as discussed previously, to convert the area integral, Eq. (5-16), to a contour integral. Applying the theorem to the drag integral we obtain:

$$\iint_H (v^2 + w^2) dS = - \int_c \phi \frac{\partial \phi}{\partial n} dc. \quad (5-18)$$

This is a general relation which converts the integral over the entire cross plane into an integral over the contour. It applies to multiple lifting surfaces. To illustrate the application of the integral to the determination of the induced drag, we consider the special case of a planar lifting surface. Here the contour integral is taken over the surface shown in Fig. 5-7, where the trace of the trailing vortices shed from the wing are contained in the slit from $-b/2$ to $b/2$.

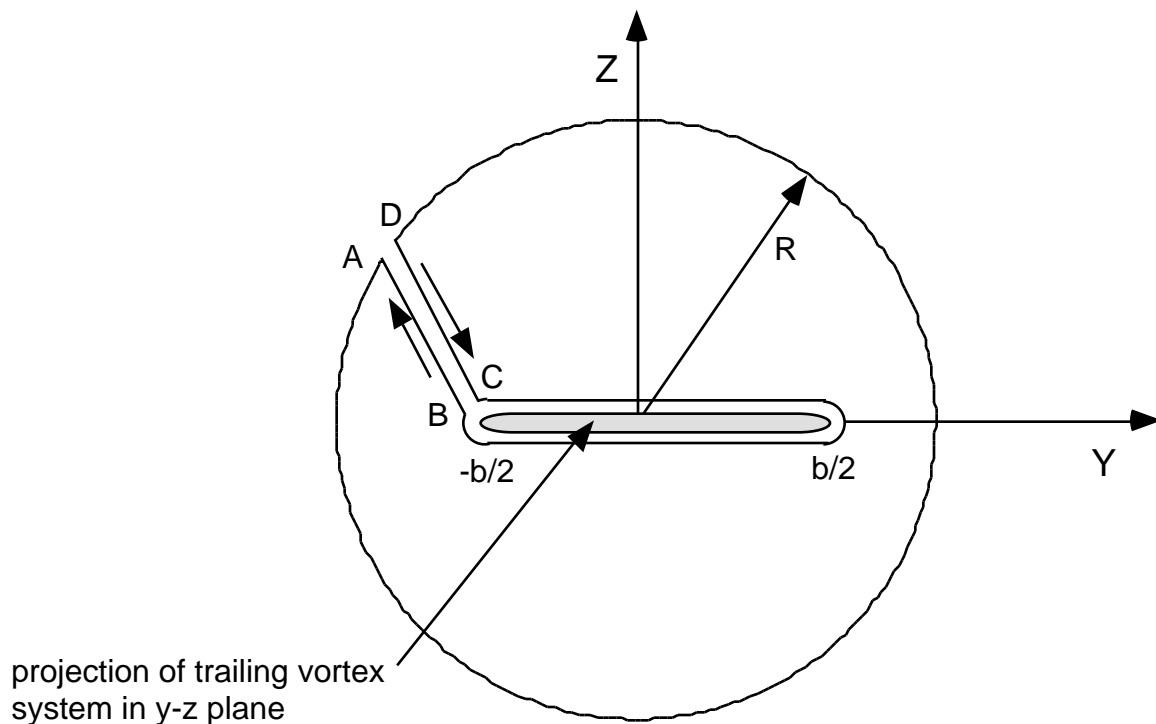


Figure 5-7. Contour integral path for induced drag analysis in the Trefftz plane.

In this *Trefftz plane*, the integral vanishes around the outside contour as $R \rightarrow \infty$ and the integrals along AB and CD cancel. Thus, the only contribution comes from the slit containing the trace of vorticity shed from the wing. The value of ϕ is equal and opposite above and below the vortex sheet, and on the sheet $\partial\phi/\partial n = w$, the downwash velocity.

Thus the integral for a single flat lifting surface can be rewritten as:

$$D_i = -\frac{1}{2} \rho_\infty \int_{-b/2}^{b/2} (\Delta\phi)_{x=\infty} w_{x=\infty} dy \quad (5-19)$$

and w is the velocity induced by the trailing vortex system. The jump in the potential on the slit at infinity can be related to the jump in potential at the trailing edge. To see this, first consider the jump in the potential at the trailing edge. Recall that the circulation is given by the contour integral:

$$\Gamma = \oint \mathbf{V} \cdot d\mathbf{s}. \quad (5-20)$$

For an airfoil we illustrate the concept by considering a small disturbance based argument. However, the results hold regardless of the small disturbance based illustration. Consider the airfoil given in Fig. 5-8.

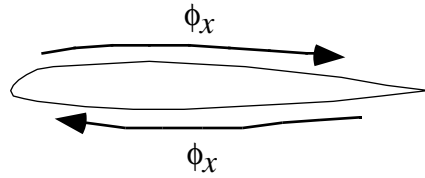


Figure 5-8. Integration path around an airfoil.

The dominant velocity is in the x -direction, $u = \phi_x$, and the integral, Eq. (5-20), around the airfoil can be seen to be essentially:

$$\begin{aligned}
 \Gamma &= \int_{TE_{lower}}^{LE} \phi_x dx + \int_{LE}^{TE_{upper}} \phi_x dx \\
 &= \phi|_{TE_{lower}}^{LE} + \phi|_{LE}^{TE_{upper}} \\
 &= \phi_{LE} - \phi_{TE_{lower}} + \phi_{TE_{upper}} - \phi_{LE} \\
 &= \phi_{TE_{upper}} - \phi_{TE_{lower}} \\
 &= \Delta\phi_{TE}
 \end{aligned} \tag{5-21}$$

The value of the potential jump at infinity can be found by realizing that the circulation is created by the wing, and any increase in the contour of integration will produce the same result.

Therefore,

$$\Delta\phi_{x=\infty} = \Delta\phi_{TE} = \Gamma(y) \tag{5-22}$$

Next, the induced velocity is found from the distribution of vorticity in the trailing vortex sheet. Considering the slit to be a sheet of vorticity, we can find the velocity induced by a distribution of vorticity from the following integral, which is a specialized case of the relation given in Chap.4, Eq.(4-42):

$$w_{x=\infty}(y) = \frac{1}{2\pi} \int_{-b/2}^{b/2} \frac{\gamma(\eta)}{y-\eta} d\eta \tag{5-23}$$

To complete the derivation we have to connect the distribution of vorticity in the trailing vortex sheet to the circulation on the wing. To do this consider the sketch of the circulation distribution given in Fig. 5-9.

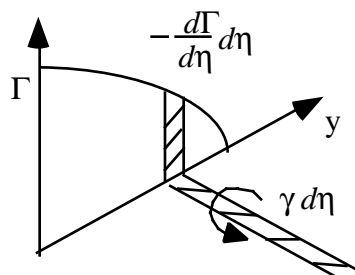


Figure 5-9. Relation between circulation change on the wing and vorticity in the wake.

As the circulation on the wing, Γ , changes across the span, circulation is conserved by shedding an amount equal to the local change into the wake. Thus the trailing vorticity strength is related to the change in circulation on the wing by

$$\gamma(\eta) = - d\Gamma/dy. \quad (5-24)$$

Substituting this into Eq. (5-23), we obtain:

$$w_{x=\infty} = -\frac{1}{2\pi} \int_{-b/2}^{b/2} \frac{d\Gamma/dy}{y-\eta} d\eta. \quad (5-25)$$

Substituting Eq. (5-22) and (5-25) into Eq.(5-19) and integrating by parts using the conditions that $\Gamma(-b/2) = \Gamma(b/2) = 0$ (which simply states that the load distribution drops to zero at the tip), we get:

$$D_i = -\frac{\rho_\infty}{4\pi} \int_{-b/2}^{b/2} \int_{-b/2}^{b/2} \frac{d\Gamma(y_1)}{dy} \frac{d\Gamma(y_2)}{dy} \ln|y_1 - y_2| dy_1 dy_2. \quad (5-26)$$

Note that this is the same form as the wave drag integral, where the area distribution is the key contributor to the wave drag, but here the spanload distribution is responsible for the induced drag. Because of the double integral we can get the total drag, but we have lost the ability to get detailed distributions of the induced drag on the body (or in the case of wave drag, its distribution on the surface). This is the price we pay to use the farfield analysis.

Finally, this result shows that the induced drag is a function of the Γ distribution (spanload) alone. Mach number effects enter only in so far as they affect the circulation distribution on the wing.

5.4 Induced Drag

Although the inviscid flow over a two-dimensional airfoil produces no drag, as we've just seen in Chapter 4, this is not true in three dimensions. The three-dimensional flowfield over a lifting surface (for which a horseshoe vortex system is a very good conceptual model) does result in a drag force, even if the flow is inviscid. This is due to the effective change in the angle of attack along the wing induced by the trailing vortex system. This induced change of angle results in a local inclination of the force vector relative to the freestream, and produces an induced drag. It is one part of the total drag due to lift, and is typically written as:

$$C_{D_i} = \frac{C_L^2}{\pi AR e}. \quad (5-27)$$

The small “ e ” in this equation is known as the span e . As we will show below, the induced drag is only a function of the spanload. Additional losses due to the fuselage and viscous effects are included when a capital E , known as Oswald's E , is used in this expression. Note that although this notation is the most prevalent in use in the US aircraft industry, other notations are frequently employed, and care must be taken when reading the literature to make sure that you understand the notation used.

When designing and evaluating wings, the question becomes: what is “ e ”, and how large can we make it? The “conventional wisdom” is that for a planar surface, $e_{max} = 1$, and for a non-planar surface or a combination of lifting surfaces, $e_{max} > 1$, where the aspect ratio, AR , is based on the projected span of the wing with the largest span.* However, studies searching for higher e 's abound. The quest of the aerodynamicist is to find a fundamental way to increase aerodynamic efficiency. In the '70s, increased aerodynamic efficiency, e , was sought by exploiting non-planar surface concepts such as winglets and canard configurations. Indeed, these concepts are now commonly employed on new configurations. In the '80s, a great deal of attention was devoted to the use of advanced wing tip shapes on nominally planar configurations. It is not clear however that the advanced wingtips result in theoretical e 's above unity. However, in practice these improved tip shapes help clean up the flowfield at the wing tip, reducing viscous effects and resulting in a reduction in drag.

To establish a technical basis for understanding the drag due to lift of wings, singly and in combination, three concepts must be discussed: farfield drag (the Trefftz plane), Munk's Stagger Theorem for design of multiple lifting surfaces, and, to understand additional drag above the induced drag due to “ e ,” it is appropriate to introduce the concept of leading edge suction. Here we will discuss the induced drag. Subsequent sections address Munk's Stagger Theorem (Section 5.6) and leading edge suction (Section 5.9)

* However, e is not *too* much bigger than unity for practical configurations.

In the last section we derived the expression for the drag due to the trailing vortex system. The far downstream location of this face of the control volume is known as the Trefftz plane. Here we explain the physical basis of the idea of the Trefftz plane following Ashley and Landahl¹⁸ almost verbatim. An alternate and valuable procedure has been described by Sears.²²

The Trefftz Plane

The idea:

1. Far downstream the motion produced by the trailing vortices becomes 2D in the y - z plane (no induced velocity in the x -direction).
2. For a wing moving at a speed U_∞ through the fluid at rest, the amount of mechanical work $D_i U_\infty$ is done on the fluid per unit time. Since the fluid is nondissipative (potential flow), it can store energy in kinetic form only. Therefore, the work $D_i U_\infty$ must show up as the value of kinetic energy contained in a length U_∞ of the distant wake.

and:

3. The vortices in the trailing vortex system far downstream can be used to find the induced drag.

The Trefftz Plane is a y - z plane far downstream, so that all motion is in the crossflow plane (y - z), and no velocity is induced in the x -direction, $u = U_\infty$. For a single planar lifting surface, the expression for drag was found to be:

$$D_i = -\frac{\rho_\infty}{4\pi} \int_{-b/2}^{b/2} \int_{-b/2}^{b/2} \frac{d\Gamma(y_1)}{dy} \frac{d\Gamma(y_2)}{dy} \ln|y_1 - y_2| dy_1 dy_2 \quad (5-26)$$

The usual means of evaluating the induced drag integral is to represent Γ as a Fourier Series,

$$\Gamma = U_\infty b \sum_{n=1}^{\infty} A_n \sin n\theta \quad (5-28)$$

The unknown values of the A_n 's are found from a Fourier series analysis, where $\Gamma(y)$ is known from an analysis of the configuration. Panel or vortex lattice methods can be used to find $\Gamma(y)$. Vortex lattice methods are described next in Chapter 6. Integration of the drag integral with this form of Γ results in:

$$D_i = \frac{\pi \rho_\infty U_\infty^2 b^2}{8} \sum_{n=1}^{\infty} n A_n^2 \quad (5-29)$$

and

$$L = \frac{\pi}{4} \rho_\infty U_\infty^2 b^2 A_1 \quad (5-30)$$

which are the classical results frequently derived using lifting line theory. Note that the lift depends on the first term of the series, whereas all of the components contribute to the drag. Putting the expressions for lift and drag into coefficient form, and then replacing the A_1 term in the drag integral by its definition in terms of the lift coefficient leads to the classical result:

$$C_{D_i} = \frac{C_L^2}{\pi A R e} \quad (5-31)$$

where:

$$e = \frac{1}{\left[1 + \sum_{n=2}^{\infty} n \left(\frac{A_n}{A_1} \right)^2 \right]} \quad (5-32)$$

These expressions show that $e_{\max} = 1$ for a planar lifting surface. However, if the slit representing the trailing vortex system is not a simple flat surface, and C_{D_i} is based on the projected span, a nonplanar or multiple lifting surface system can result in values of $e > 1$. In particular, biplane theory addresses the multiple lifting surface case, see Thwaites²³ for a detailed discussion. If the wing is twisted, and the shape of the spanload changes as the lift changes, then e is not a constant, independent of the lift coefficient.

It is important to understand that the induced drag contribution to the drag due to lift assumes that the airfoil sections in the wing are operating perfectly, as if in a two-dimensional potential flow that has been reoriented relative to the freestream velocity at the angle associated with the effects of the trailing vortex system. Wings can be designed to operate very close to these conditions.

We conclude from this discussion:

1. Regardless of the wing planform(s), induced drag is a function of circulation distribution alone, independent of Mach number except in the manner which Mach number influences the circulation distribution (a minor effect in subsonic/transonic flow).
2. Given Γ , “ e ” can be determined by finding the A_n ’s of the Fourier series for the simple planar wing case. Other methods are required for nonplanar systems.
3. Extra drag due to the *airfoil’s* inability to create lift ideally must be added *over and above* the induced drag (our analysis here assumes that the airfoils operate perfectly in a two-dimensional sense; there is no drag due to lift in two-dimensional flow).

5.5 Program LIDRAG

For single planar surfaces, a simple Fourier analysis of the spanload to determine the “ e ” using a Fast Fourier Transform is available from the code **LIDRAG**. The user’s manual is given in Appendix D.3. Numerous other methods could be used. For reference, note that the “ e ” for an elliptic spanload is 1.0, and the “ e ” for a triangular spanload is 0.728. **LIDRAG** was written by Dave Ives, and is employed in numerous aerodynamics codes.²⁴

5.6 Multiple Lifting Surfaces and Munk's Stagger Theorem

An important result in the consideration of multiple lifting surfaces is Munk’s Stagger Theorem.²⁵ It states that the *total* induced drag of a multi-surface system does not change when the elements of the system are translated parallel to the direction of the flow, as illustrated in the sketch shown in Fig. 5-10, *provided* that the circulation distributions on the elements are left unchanged. This theorem is proven in the text by Milne-Thompson.²⁵ Thus the drag depends only on the projection of the system in the cross-plane. This means that given the circulation distributions, the Trefftz plane analysis can be used to find the induced drag. This is consistent with the analysis given for the Trefftz plane above, and reinforces the concept of using the farfield analysis to determine the induced drag. Naturally, to maintain the circulation distribution of the elements when they are repositioned their geometric incidence and twist have to be changed.

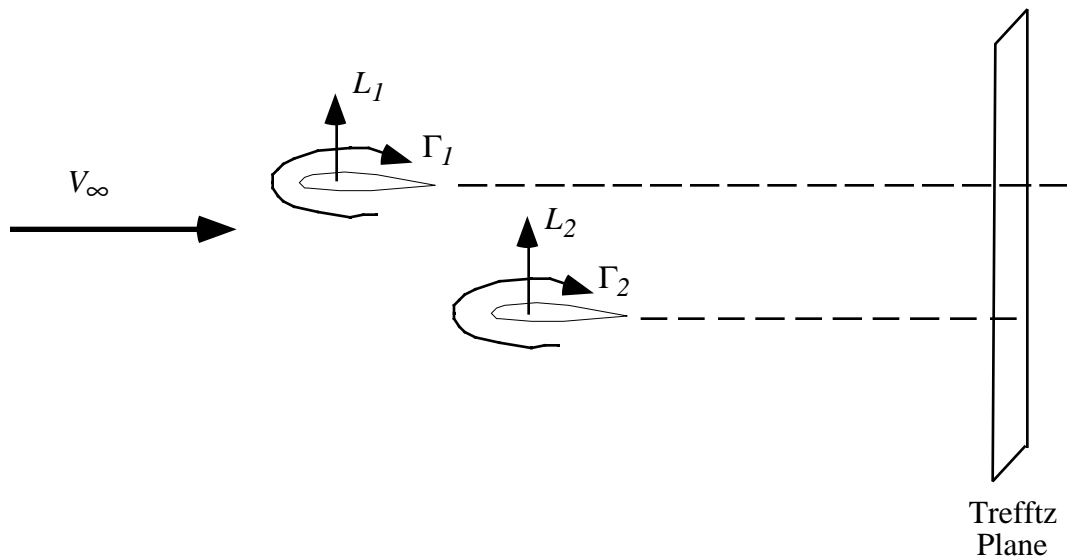


Fig. 5-10. Example of Munk’s Stagger Theorem, where the fore and aft positions of multiple lifting surfaces do not affect drag as long as the circulation distribution remains fixed.

When the lifting system is not limited to a single lifting component, **LIDRAG** cannot be used to find the span e . However, two limiting cases can be considered. If the lifting elements are in the same plane, then the sum of the spanloads should be elliptic for minimum drag. If the elements are vertically separated by a large distance, then each component individually should have an elliptic spanload to obtain minimum induced drag.

When the system is composed of two lifting surfaces, or a lifting surface with dihedral breaks, including winglets, then a code by John Lamar²⁶ is available to analyze the induced drag. As originally developed, this code finds the minimum induced drag and the required spanloads for a prescribed lift and pitching moment constraint. It is known as **LAMDES**, and the user's manual is given in Appendix D.4. This program is much more elaborate than **LIDRAG**. For subsonic flow the program will also estimate the camber and twist of the lifting surfaces required to achieve the minimum drag spanload. I extended this code to incorporate, approximately, the effects of viscosity and find the system e for a user supplied spanload distribution.²⁷

5.7 Zero Lift Drag Friction and Form Drag Estimation

Although not formally part of computational aerodynamics, estimates of skin friction based on classical flat plate skin friction formulas can be used to provide initial estimates of the friction and form drag portion of the zero lift drag. These are required for aerodynamic design studies using the rest of the methods described here. These simple formulas are used in conceptual design in place of detailed boundary layer calculations, and provide good initial estimates until more detailed calculations using the boundary layer methods described in Chapter 10 are made. They are included here because they appear to have been omitted from current basic aerodynamics text books.* An excellent examination of the methods and accuracy of the approach described here was given by Paterson, MacWilkinson and Blackerby of Lockheed.²⁸

For a highly streamlined, aerodynamically clean shape the zero lift drag (friction and form drag at subsonic speeds where there are no shock waves) should be mostly due to these contributions, and can be estimated using skin friction formulas. However, Table 5-1, for a typical military attack airplane, shows that on this airplane only about two-thirds of the zero lift drag is associated with skin friction and form drag. This illustrates the serious performance penalties associated with seemingly small details. R.T. Jones²⁹ has presented a striking figure, included here as Fig. 5-11, comparing the drag on a modern airfoil to that of a single wire. It's hard to believe, and demonstrates the importance of streamlining. An accurate drag estimate requires that these details be included in the estimates.

* Expanded details including compressibility effects and mixed laminar-turbulent skin friction estimates are given in App. D.5, FRICTION.

Fig. 5-11. A wire and airfoil with the same drag!²⁹

Until recently, aerodynamicists assumed the flow was completely turbulent. However, as a result of work at NASA over the last decade and a half, some configurations can now take advantage of at least some laminar flow, with its significant reduction in friction drag. Advanced airfoils can have as much as 30 to 40% laminar flow.

As an example of this approach, consider a typical turbulent flow skin friction formula (for one side of a “flat plate” surface only):

$$C_F = \frac{1.455}{[\log \text{Re}_c]^{2.58}} \quad (5-33)$$

where “log” means log to the base 10. Note also that the capital C_F denotes an integrated value. Formulas for the local skin friction coefficient customarily use a small f subscript.

Numerous form factors are available to help account for effects due to thickness and additional trailing edge pressure drag. Hoerner⁹ and Covert⁸ provide summaries. For planar surfaces, one form factor is,

$$FF = 1 + 1.8 \left(\frac{t}{c} \right) + 50 \left(\frac{t}{c} \right)^4 \quad (5-34)$$

where t/c is the maximum thickness to chord ratio. For bodies, the form factor would be:

$$FF = 1 + 1.5 \left(\frac{d}{l} \right)^{1.5} + 7 \left(\frac{d}{l} \right)^3 \quad (5-35)$$

where d/l is the diameter to length ratio. The skin friction coefficient estimate is then converted to aircraft coefficient form through:

$$C_{D0} \cong C_F \frac{S_{wet}}{S_{ref}} FF \quad (5-36)$$

Here S_{wet} is the total area scrubbed by the flow, and S_{ref} is the reference area used in the definition of the force coefficients. For a thin wing the reference area is usually the planform area and the wetted area is approximately twice the planform area (including the upper and lower surface of the wing).

Program **FRICITION** automates this procedure using slightly improved formulas for the skin friction that include compressibility effects. The program computes the skin friction and form drag over each component, including laminar and turbulent flow. The user can input either the Mach and Reynolds numbers or the Mach number and altitude. The use of this program is described in Appendix D.5. This analysis assumes that the aircraft is highly streamlined. For many aircraft this is not the case. As discussed above, Table 5-1 provides an example of the significantly increased drag that results when developing an aircraft for operational use.

Comment: On a tour of the final assembly lines of the Boeing 747 and 777 on February 29, 1996, I observed that the 777 was much, much smoother aerodynamically than the 747. Clearly, a lot of the advanced performance of the 777 is due to old-fashioned attention to detail. The aerodynamicists have apparently finally convinced the manufacturing engineers of the importance of aerodynamic cleanliness. Think about this the next time you compare a Cessna 182 to the modern homebuilts, as exemplified by the Lancairs and Glassairs.

More details are presented in Chapter 10, Viscous Flows in Aerodynamics. Viscous effects due to lift and shock-wave boundary layer interaction are also discussed in Chapter 11, Transonic Aerodynamics.

Table 5-1
Example of zero lift drag buildup on a “dirty” military airplane.

Low Speed Minimum Parasite Drag Breakdown
 $M < .65, C_L = 0.0$

<u>Component</u>	S_{wet}	S_π	C_{Df}	$C_{D\pi}$	ΔC_D	<u>% Total</u>
1 Wing						22.1%
a) not affected by slats	262.		.00308		.00308	
b) not affected by slats	150.		.00280		.00162	
2. Horizontal Tail	84.4		.0033		.00108	5.1%
3. Vertical Tail	117.		.00385		.00173	8.1%
4. Fuselage (including inlets)	434.		.00306		.00512	24.0%
5. Enclosure		2.3		.122	.00108	5.1%
6. Appendages						33.1%
a) Upper avionics bay					.00069	
b) Drag-chute fairing					.00012	
c) Landing gear fairings					.00042	
d) Aero 7A Rack-Pylon @ CL					.00058	
e) Arresting hook					.00058	
f) Inflight-Fueling Probe					.00092	
g) Wing-Vortex Generators					.00115	
h) Boundary Layer Diverter					.00042	
i) Boundary-Layer Splitter Plate					.00004	
j) Inlet Vortex Fences					.00023	
k) Landing Spoilers					.00012	
l) ECM Antenna and Chaff Dispensers					.00038	
m) Pitot tube					.00004	
n) Angle-of-Attack Indicator					.00004	
o) Rudder Damper					.00023	
p) Aileron Damper					.00023	
q) Barrier Detents					.00008	
r) Anti-Collision Lights					.00008	
s) Radar altimeter					.00015	
t) Fuel Dump and Vent					.00023	
u) Airblast Rain Removal					.00008	
v) Catapult Holdback					.00027	
7. Inlets and Exits						
a) Powerplant (vents, etc.)					.00027	1.6%
b) Air Conditioning					.00008	
8. Miscellaneous					.00020	.9%
Total Zero lift drag coefficient (based on $S_{ref} = 260 \text{ ft}^2$)					.0213	100.0%

Note: based on a total wetted area of 1119 ft^2 , $C_D = .00495$

5.8 Supersonic Wave Drag: The Farfield Wave Drag Integral and the Area Rule

The farfield analysis also showed us that for supersonic flight there is a wave drag. Not surprisingly, the supersonic wave drag has played a key role in the aerodynamic design of supersonic aircraft. The equations are repeated here as:

$$\bar{D}_w(\theta) = -\frac{\rho_\infty U_\infty^2}{4\pi} \int_0^l \int_0^l S'''(x_1) S'''(x_2) \ln|x_1 - x_2| dx_1 dx_2 \quad (5-12)$$

and

$$D_w = \frac{1}{2\pi} \int_0^{2\pi} \bar{D}_w(\theta) d\theta \quad (5-13)$$

where the $S(x)$ values represent the area from an oblique (Mach angle) cut to find the cross section area of the aircraft at a specific theta.

The importance of the distribution of the cross-sectional area is clear in the integral. To minimize the integral the area change should be very smooth. Thus, the shaping of the design geometry plays a major role in the value of the integral. In any case, low drag is achieved by minimizing the maximum cross-sectional area of the design. The key parameter is the fineness ratio, which is the length divided by the maximum diameter. Increasing the fineness ratio decreases the wave drag. A number of minimum drag bodies of revolution have been derived using Eq. (5-12). The geometric details of these shapes are given in Appendix A.

The principle that aerodynamicists use to achieve low values of wave drag is known as the *area rule*. Proposed by Richard Whitcomb* at the NACA's Langley Field, the area rule states that the air displaced by the body should develop in a smooth fashion as it moves around and along the body, with no sudden discontinuities. Thus the total aircraft area distribution should form a smooth progression. In particular, when the wing becomes part of the cross-sectional area, the adjacent fuselage area should be reduced to make the total area distribution smooth. This results in the distinctive area ruled, or "coke bottle," fuselage shape.

Whitcomb's evidence for the validity of this rule was obtained experimentally (the computer had not yet become practical design tool). Figure 5-12 shows the key result obtained by Whitcomb.³⁰ The increase in drag with increasing transonic Mach number is almost identical for a wing-body combination and a body of revolution with the same cross sectional area distribution. The wing-body combination has significantly higher subsonic drag because of the increased surface area compared to the body alone case. All the cases Whitcomb presented weren't as dramatic, but similar trends were found for a number of shapes. Whitcomb's original idea addressed

* He won the Collier trophy for this work.

transonic speeds, and the normal area distribution (the area in the plane perpendicular to the flow) was made smooth to obtain low drag. At supersonic speeds the problem is more complicated. Instead of using the normal area distribution, the supersonic area rule requires that the area on the so-called Mach cuts that correspond to the area distribution along the Mach angle for each theta angle (Eq. 5-13) be smooth.

Figure 5-12. Whitcomb's proof of the area rule.³⁰

The most famous application of the area rule occurred on the F-102 aircraft program.* This airplane was supposed to be supersonic in level flight. When it first flew, the prototype YF-102 was unable to break the sound barrier and fly supersonically. The nose was lengthened approximately five feet and area was added (with the plane already completed it was impossible to remove area) to the fuselage via faired bulges—or “bustles”—at the wing trailing edge-fuselage intersection. The bulges were faired beyond the engine exhaust nozzle to improve the fineness ratio and area distribution. After these modifications, the prototype YF-102 was capable of penetrating deeper into the transonic region. However, it was still not capable of exceeding Mach 1.0 in level flight. A complete redesign was necessary. It had to be done to continue the contract.

* Portions of this section were contributed by Nathan Kirschaum.

One hundred and seventeen working days later(!), a new, completely redesigned F-102 was ready to fly. The fuselage fineness ratio and area distribution had been increased and refined. The fuselage mid-section cross-sectional area had been reduced (cinched-up, wasp waisted, or coke-bottled) as much as structure and component integration would permit. It was lengthened 11 feet 3 inches, with most of the increased length added ahead of the wing. The cockpit canopy was reduced in cross-section with a near triangular cross-section and headed by a flat plate, highly swept “V” windshield. The cockpit and the side-mounted engine inlets were moved forward to reduce their sudden area build-up, or impact on the fuselage area. The aft fuselage bustles were retained to avoid the rapid collapse of the cross-sectional area at the delta wing trailing edge. So reconfigured, the airplane was able to fly at low supersonic speeds ($M = 1.2$). Figure 5-13 shows the original prototype and the reconfigured F-102A as produced for service use.³¹ The resulting change in drag from the YF-102 to the F-102A was about twenty-five counts, and is shown in Fig. 5-14 (from the original Convair plot). Although the change might not appear dramatic, the reduction in wave drag was sufficient to allow the plane to fly faster than the speed of sound. Notice also that the use of conical camber (discussed later), introduced to improve the lift and drag due to lift characteristics of the delta wing, added a significant penalty (camber drag) to the minimum drag.

Subsequently, the configuration was completely redesigned incorporating a more refined, integrated area rule. Further slimmed down by a reduced weapon bay capacity and shortened and repositioned engine air intake ducts, and powered by a fifty percent more powerful engine, it was capable of routine Mach 2+ speeds. The designation was then changed to F-106A. This design is also shown in Fig. 5-13. The volume of the increased area of the vertical tail on the F-106A, required to counteract the loss of tail surface effectiveness at the increased operational Mach number, replaced the aft side “bustles” on the F-102.

As an historical note, the Grumman F-11F (F-11) was the first aircraft designed “from scratch” using the area rule. The result is clearly evident as shown in Fig. 5-15a.³² Another design employing the area rule in an effective manner was the Northrop F-5A/B (and the T-38 derivative), as shown in Fig. 5-15b.³² This design had essentially unswept wings. Even the wing tip fuel tanks were area ruled, although the inboard localized area reduction could be arguably assigned to Küchemann interface contour theorems.¹⁴

When considering the area rule, remember that this is only one part of successful airplane design.³³ Moreover, extreme area ruling for a specific Mach number may significantly degrade the performance of the design at other Mach numbers.

Figure 5-13 Convair YF-102, F-102A, F-106A configuration evolution.³¹

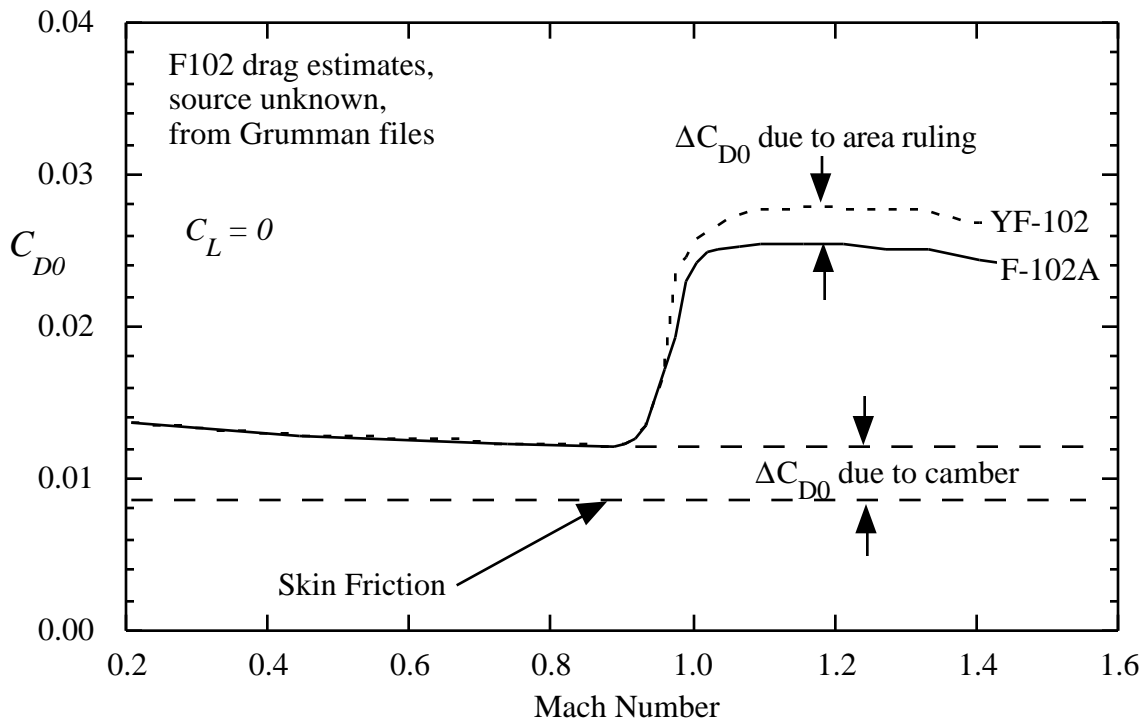


Figure 5-14. Zero lift drag for the YF-102 and F-102A airplanes.

To estimate the wave drag, a theoretical analysis of the integral is available.* Note that the integrand is proportional to the second derivative of the area distribution, so that even without an analysis it is clear that the lowest drag occurs when the distribution is made as smooth as possible. Eminton³⁴ devised the standard method for the numerical evaluation of the integral in Eqn. 5-12. The difficulty in evaluating the integral is that the result depends on the second derivative of the area distribution. This distribution is made up of contributions from numerous components, and it is not known with great precision. Polynomials or other interpolation schemes used to perform the quadrature may amplify any imprecision in the data, and produce unreasonably high drag predictions. Ms. Eminton used a Fourier series for the distribution of the gradient of the area. The coefficients are then found by solving an optimization problem that determines the coefficients that will produce the curve passing through the known values of the area having the least drag. In this sense the method is also a design method. By specifying a small number of control stations (say, from a designer's configuration layout) with a specified area distribution, the method will provide the complete distribution of area required for minimum drag and satisfying the imposed control station constraints.

* Note: advanced CFD calculation methods don't require the aerodynamicist to look at the problem using the area rule diagram. Those approaches don't provide the insight for design available through the area rule diagram.

a) Grumman F-11F

b) Northrop F-5A/B

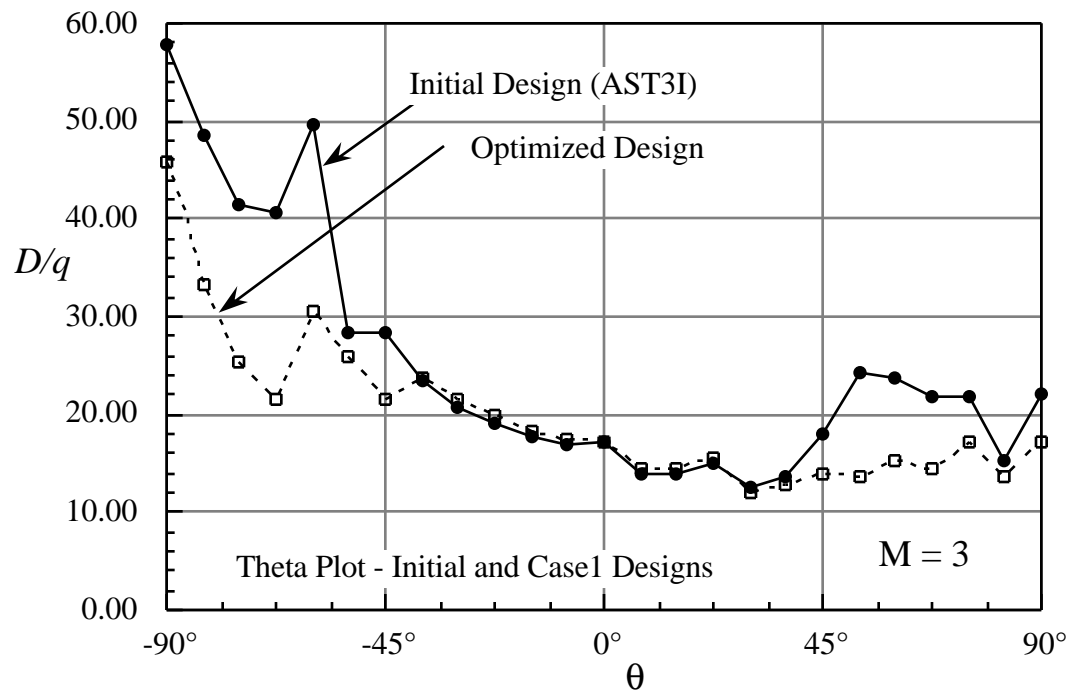
Figure 15. Other aircraft designs with evident area ruling.

The practical implementation of this scheme is available in the so-called Harris wave drag program.²¹ Figure 5-16 illustrates the procedure. At each “roll angle” θ a number of x -cuts are made to use in evaluating the integral. Typically, 50 to 100 x -cuts are made for each of from 24 to 36 θ values. Note that in making these calculations the inlet capture area is removed from the area distribution.

As discussed above, area ruling plays an important role in supersonic cruise vehicle design. Figure 5-17 presents the results of an analysis of a current high speed civil transport (HSCT) concept.³⁵ Figure 5-17a shows the highly blended configuration. Figure 5-17b shows the variation in drag as the integral is computed for various “theta cuts.” This curve also contains the results of a combined structural-aerodynamic study to improve this design using systematic advanced design methodology.³⁶ Note that the drag is presented in terms of D/q . This is a traditional approach, and eliminates any false impressions produced when configurations with differing reference areas are compared. Figure 5-17c shows the normal area distribution. Here the nacelles are seen to make a large impact on the area distribution. However, the area distribution of interest is for $M = 3.0$. Figures 5-17d and e present the area distributions for the theta 0° and 90° cases. Here the area distribution is seen to be much smoother. This is especially true for the theta 0° case. The theta 90° case still shows the problem of integrating the propulsion system into the configuration to obtain a smooth area distribution. Comparing the area distributions presented in Figures 5-17d and 17e with the change in drag at these two different roll angles provides some insight into the importance of shaping to produce a smooth area distribution.

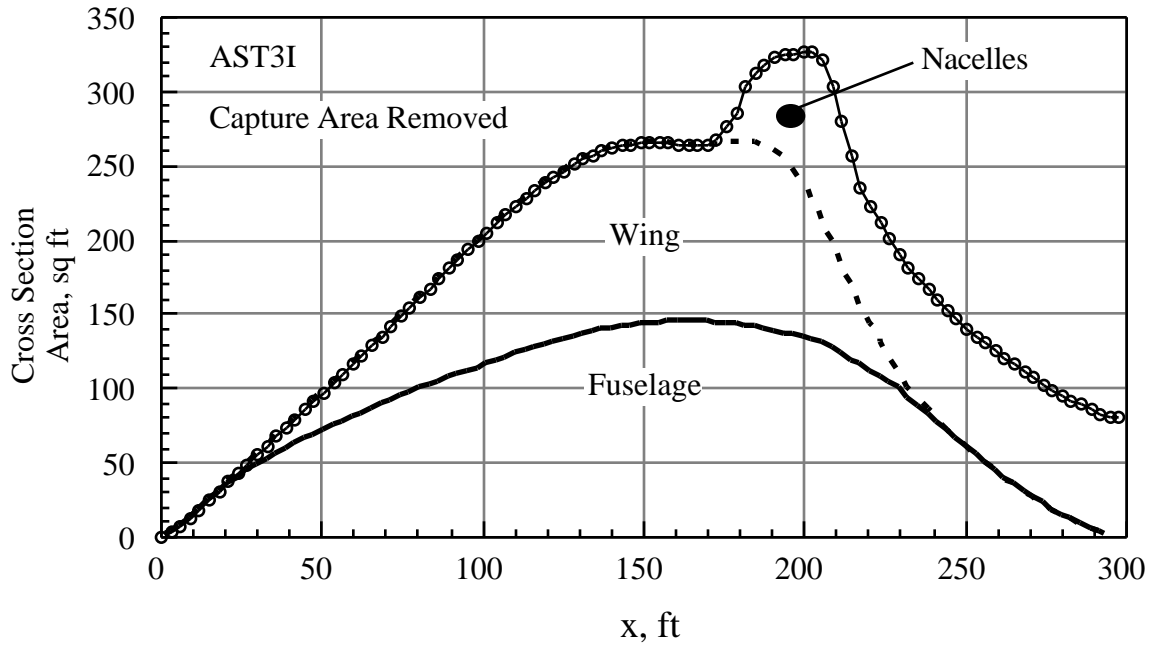
Figure 5-16 Evaluation of the wave drag integral.²¹

a) basic concept three view

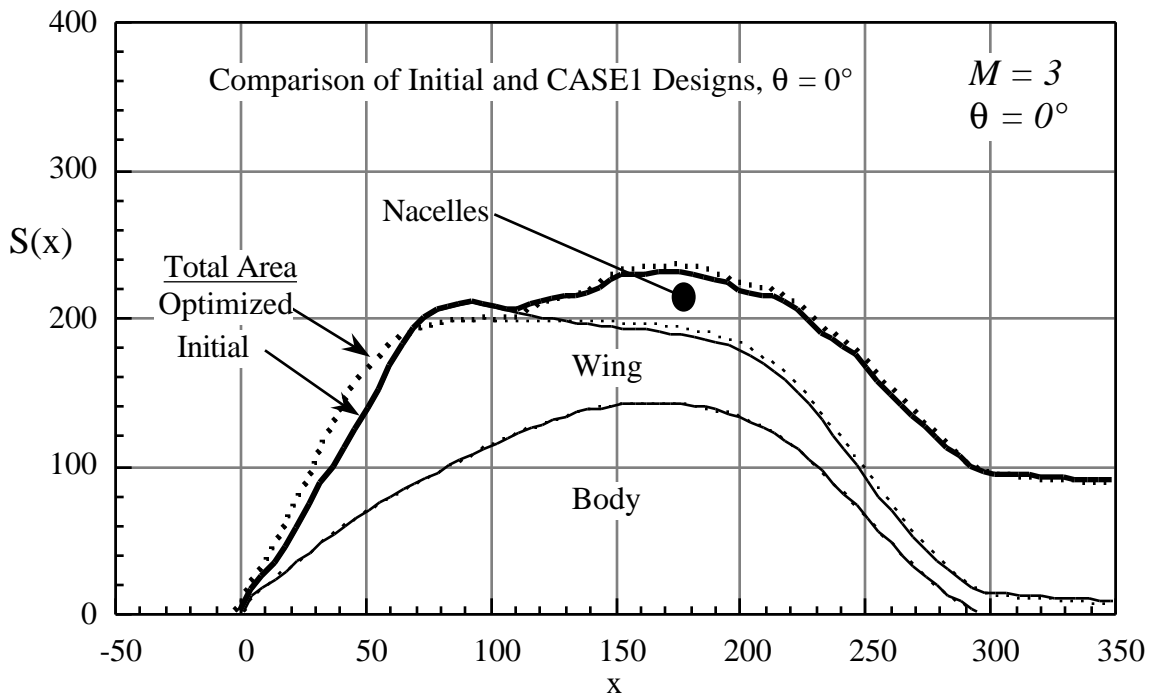


b) distribution of the drag for each circumferential cut.

Figure 5-17 The AST3I,³⁵ an advanced concept for a Mach 3 High Speed Civil Transport.



c) normal area distribution (capture area removed)



d) Mach 3 area distribution, $\theta = 0^\circ$

Figure 5-17 The AST3I,³⁵ an advanced Mach 3 High Speed Civil Transport (cont'd).

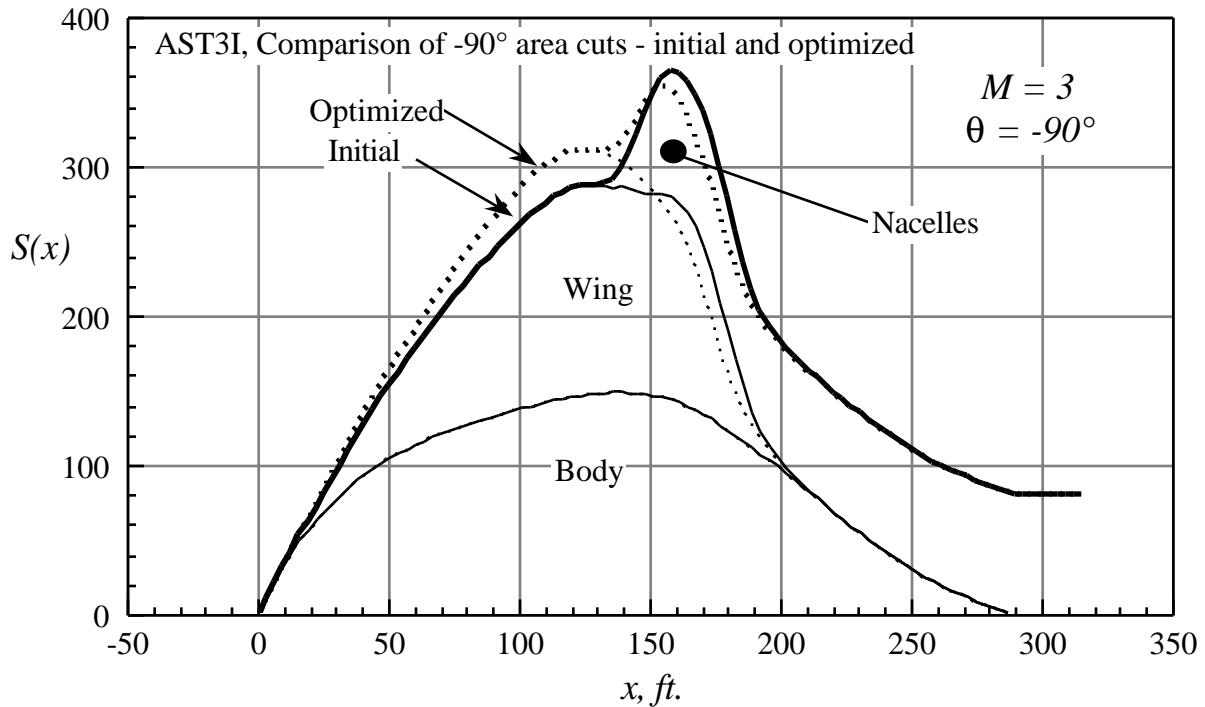
e) Mach 3 area distribution, $\theta = 90^\circ$

Figure 5-17 The AST3I,³⁵ an advanced Mach 3 High Speed Civil Transport (concluded).

Area diagrams for typical current fighters are not nearly so streamlined. Figure 5-18 shows the area distribution for the F-16.³⁷ The original area distribution is seen in Fig. 5-18a, and the result of refinements in Fig 5-18b. The F-16 was not designed primarily for supersonic flight, and it has a low fineness ratio and consequently a relatively high wave drag. Small aircraft are much more difficult to lay out to ensure a smooth distribution of area. Note in Fig. 5-18 that the canopy is placed to help “fill in” the area diagram. Figure 5-18b shows the revisions made to improve the contour forward and aft of the maximum cross-sectional area to fill in the shape and also add fuel volume. Note that this curve has no scale. Manufacturers are sensitive about this information.

There is also a wave drag due to lift (see Ashley and Landahl¹⁸). However, almost all area ruling at supersonic speeds primarily emphasizes the volumetric wave drag.

a) Original cross-sectional area

b) Refined area distribution

Figure 5-18 The YF-16 area rule diagram.³⁷

5.9 The Leading Edge Suction Concept

Aerodynamicists often evaluate the performance of configurations in term of so-called leading edge suction. The concept can be explained by considering the inviscid flow over the proverbial zero thickness flat plate at angle of attack in an incompressible inviscid flow, as shown in Fig. 5-19.

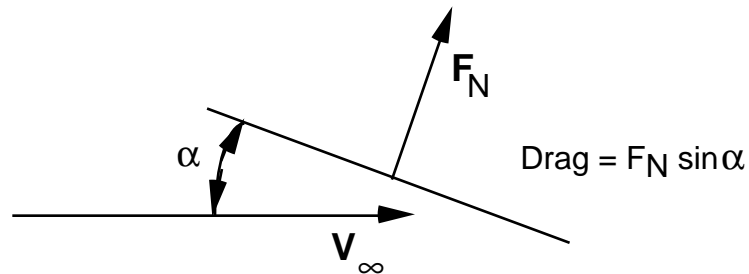


Figure 5-19 Basic relations between forces for an infinitely thin plate.

What is the drag? According to theory, it must be zero. In the sketch we see that the force acts in a direction perpendicular to the plate, and this clearly leads to a force component in the drag direction. What's the explanation of the paradox? Consider the following sketch of the front portion of an airfoil section in Fig. 5-20.

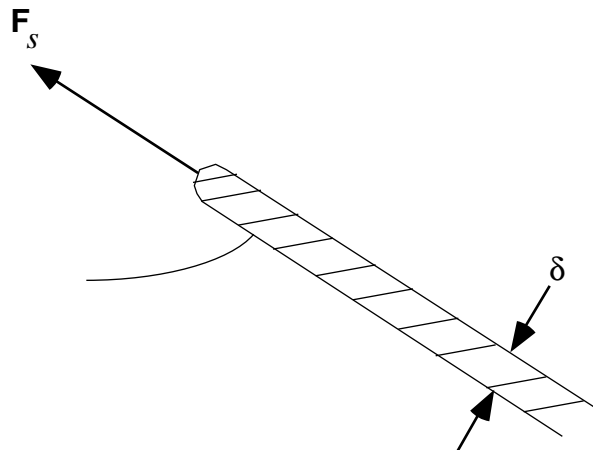


Figure 5-20. Details of the flow near the leading edge of a thin plate.

There is a low pressure over the front edge face due to the expansion of the flow around the leading edge. The expansion becomes stronger as the thickness decreases, so that the force on the front face of the plate due to the product of the pressure and plate thickness is:

$$F_s = \lim_{\delta \rightarrow 0} (\delta \cdot C_{p_s} q_\infty) = \text{finite} \quad (5-37)$$

and the value of the limit is just such that the drag is zero. Thus the correct model of the flow over the flat plate is actually modified from the sketch given above to include an edge force, as shown in Fig. 5-21.

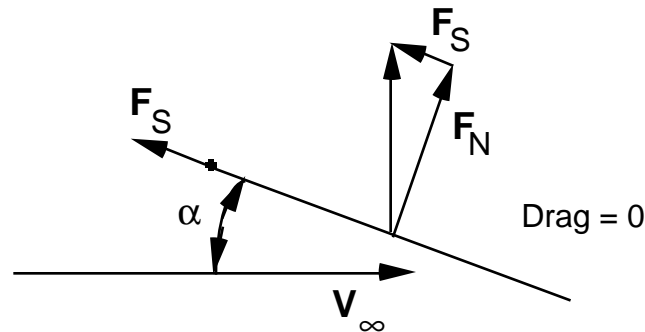


Figure 5-21. Corrected flow model to satisfy inviscid flow theory.

Of course, a very thin flat plate will realize almost none of the suction force, and hence will have a drag component. However, an airfoil section (even a fairly thin one) with a smooth round nose may in fact achieve nearly all of the suction force, at least at small angles of attack. If the airfoil section in the wing does not achieve the full suction performance, the resulting drag must be added to the induced drag.

The drag due to lift is thus broken up into induced drag and additional profile drag. As described previously, the induced drag is a function of the wing spanload only, and is independent of the details of the particular airfoil used in the wing. The additional profile drag is associated with the airfoil used in the wing. At low lift coefficients this drag should be small, only becoming important as flow separation starts to develop on the airfoil section. The additional profile drag becomes large as wing stall is approached.

Wing performance is evaluated based on the ability to obtain a high value of the lift to drag ratio, (L/D), relative to the maximum possible for that planform, and the ability to achieve a high maximum lift coefficient. Essentially, the wing is designed to allow the airfoil to achieve its full performance. Recalling that a two-dimensional airfoil under the assumption of inviscid subsonic flow has no drag due to lift, the maximum performance should occur by adding the induced drag, assuming an elliptic spanload, to the zero lift drag. This is known as the 100% suction polar, since the airfoil section has no additional profile drag due to lift, and is thus achieving 100% of the leading edge suction required to eliminate the drag force in a two-dimensional flow. This lift is

$$C_{DL100\%} = C_L^2 / \pi AR. \quad (5-38)$$

At the other extreme, the worst case occurs when the airfoil fails to produce any efficient lift, such that the only force is normal to the surface and there is no edge or suction* force (0% leading edge suction). In this case the entire lifting force on the wing is the normal force, and the polar can be determined by resolving that force into lift and drag components. The equation for the 0% suction drag can be expressed in a variety of forms, starting with

$$C_{DL0\%} = C_L \tan(\alpha - \alpha_0) \quad (5-39)$$

where α_0 is the zero lift angle of attack. We also use the linear aerodynamic relation:

$$C_L = C_{L\alpha} (\alpha - \alpha_0) \quad (5-40)$$

which can be solved for the angle of attack:

$$(\alpha - \alpha_0) = \frac{C_L}{C_{L\alpha}} \quad (5-41)$$

Finally, substitute Eqn. (5-41) into Eqn. (5-39) for the angle of attack as follows:

$$\begin{aligned} C_{DL0\%} &= C_L \tan(\alpha - \alpha_0) \cong C_L (\alpha - \alpha_0) \\ &\cong C_L \frac{C_L}{C_{L\alpha}} \end{aligned}$$

or

$$C_{DL0\%} \cong \frac{C_L^2}{C_{L\alpha}} \quad (5-42)$$

This equation for the 0% suction polar shows why this polar is often referred to as the “ $1/C_{L\alpha}$ ” polar by aerodynamicists. Using this approach, effective wing performance is quoted in terms of the fraction of suction achieved, based on the difference between the actual drag and the 100% and 0% suction values as shown in Figure 5-22. This figure illustrates how wings typically perform. The wing will approach the 100% level at low lift coefficients, and then as flow separation starts to develop, the performance deteriorates. Eventually, the wing may have a drag substantially higher than the 0% suction value that was said above to be the worst case.

* On a swept wing the suction force is normal to the leading edge. The component of the leading edge suction force in the streamwise direction is called the leading edge thrust.

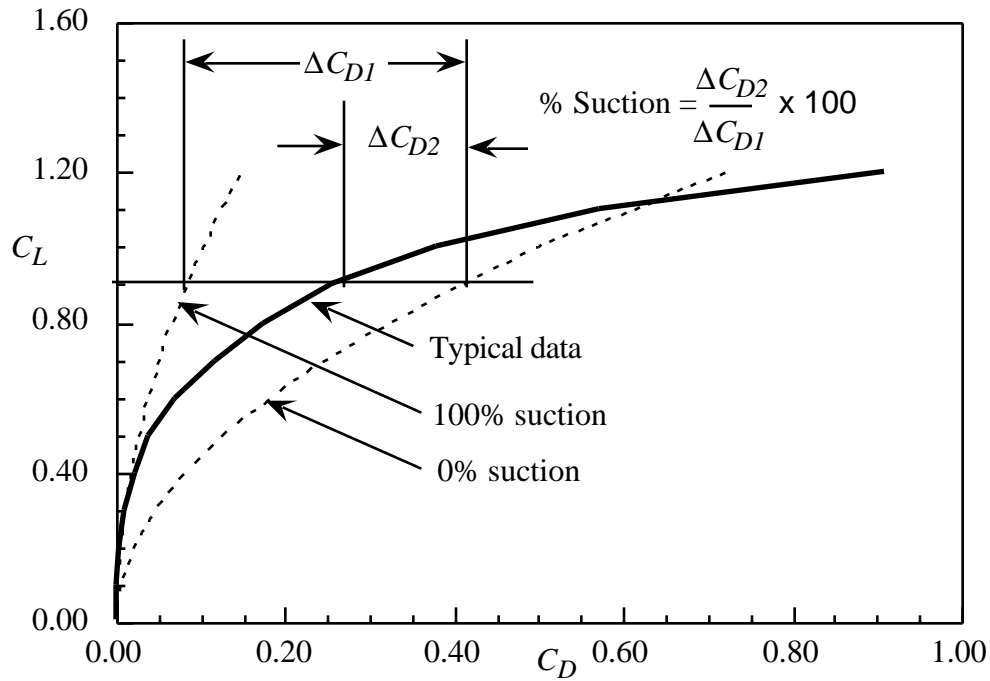


Figure 5-22 Definition of percent leading edge suction performance.

The value of E for this level of performance can be found by equating Eq.(5-42) to the standard form:

$$C_{DL} = \frac{C_L^2}{\pi A R E} \tag{5-43}$$

which leads to:

$$E_{0\%} = \frac{C_{L\alpha}}{\pi A R} . \tag{5-44}$$

Typically, the value of E varies with the lift coefficient. By plotting experimental data, typical variations can be obtained for various classes of wings. Figure 5-23 shows the typical variation. This relation was shown in general by McKinney and Dollyhigh.³⁸

Alternately, in supersonic flow, the drag due to lift relation is frequently written as

$$C_{DL} = K C_L^2 \tag{5-45}$$

for uncambered airfoils. For cambered and twisted wings the polar is shifted, and the minimum drag occurs at a C_L other than zero, as shown previously in Fig. 5-2, and described by Eq. (5-2). In practice we expect the wing to achieve a performance level between the $K_{100\%}$ and $K_{0\%}$ limits. This approach is described in detail by Raymer.³⁹

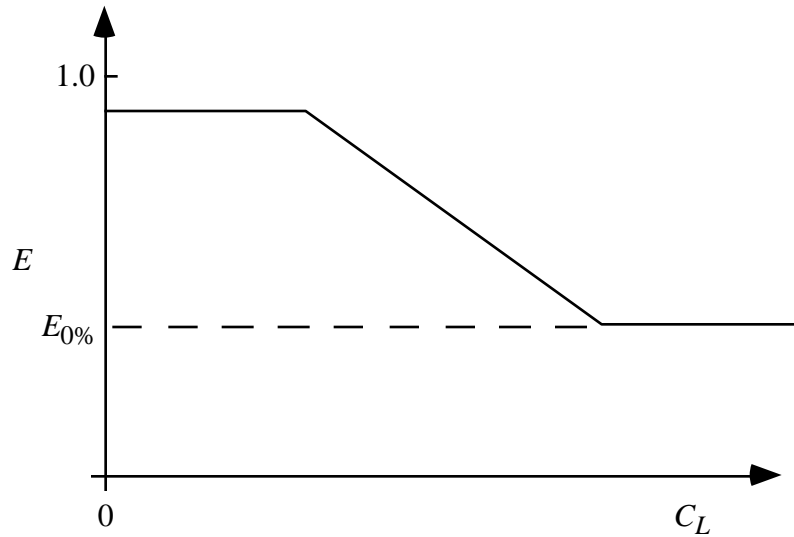


Figure 5-23. Typical variation of E with lift coefficient.

In considering the shift of the polar, a few comments are required. First, the wing performance cannot exceed the optimum value, which for subsonic flow over a single planar lifting surface is $E = 1$. Especially for wings in supersonic flow it is hard to get 100% of the leading edge suction. In that case the approach is to camber the wing to make the drag performance of a wing with less than 100% suction attain the 100% suction level at a specified value of lift, C_{LD} . Using the polar definition

$$C_D = \Delta C_{D_m} + K_{xx\%} (C_L - C_{L_m})^2 \quad (5-46)$$

where the value of K corresponds to the performance of the wing in terms of leading edge suction (LES), we find the values of ΔC_{D_m} and C_{L_m} in terms of the design lift, C_{L_d} . To do this equate the polar to the 100% suction value at the design lift. This polar must also be tangent to the 100% polar at this point so that the polar will not predict better performance than the optimum at other values of the lift. Using as an example a 0% leading edge suction wing:

$$C_D(100\% \text{ LES}) = C_D(0\% \text{ LES}) \Big|_{C_L=C_{L_d}} \quad (5-47)$$

$$\frac{dC_D(100\% \text{ LES})}{dC_L} = \frac{dC_D(0\% \text{ LES})}{dC_L} \Big|_{C_L=C_{L_d}} \quad (5-48)$$

and the unknown values of ΔC_{D_m} and C_{L_m} are:

$$C_{L_m} = \left(1 - \frac{K_{100\%}}{K_{0\%}} \right) C_{L_d} \quad (5-49)$$

and

$$\Delta C_{D_m} = K_{100\%} C_{L_d}^2 - K_{0\%} (C_{L_d} - C_{L_m})^2. \quad (5-50)$$

In any experimental evaluation of wing performance both the 100% and 0% polars should be constructed, and used to establish bounds on the experimental polar. Thus a typical drag polar would include the 100% and 0% suction polars as well as the predicted or measured performance to establish a basis for evaluating a wing's efficiency. Figure 5-24 presents the actual performance of an unswept rectangular wing at subsonic speed. Here the performance is very close to the lower drag limit until the wing stalls.

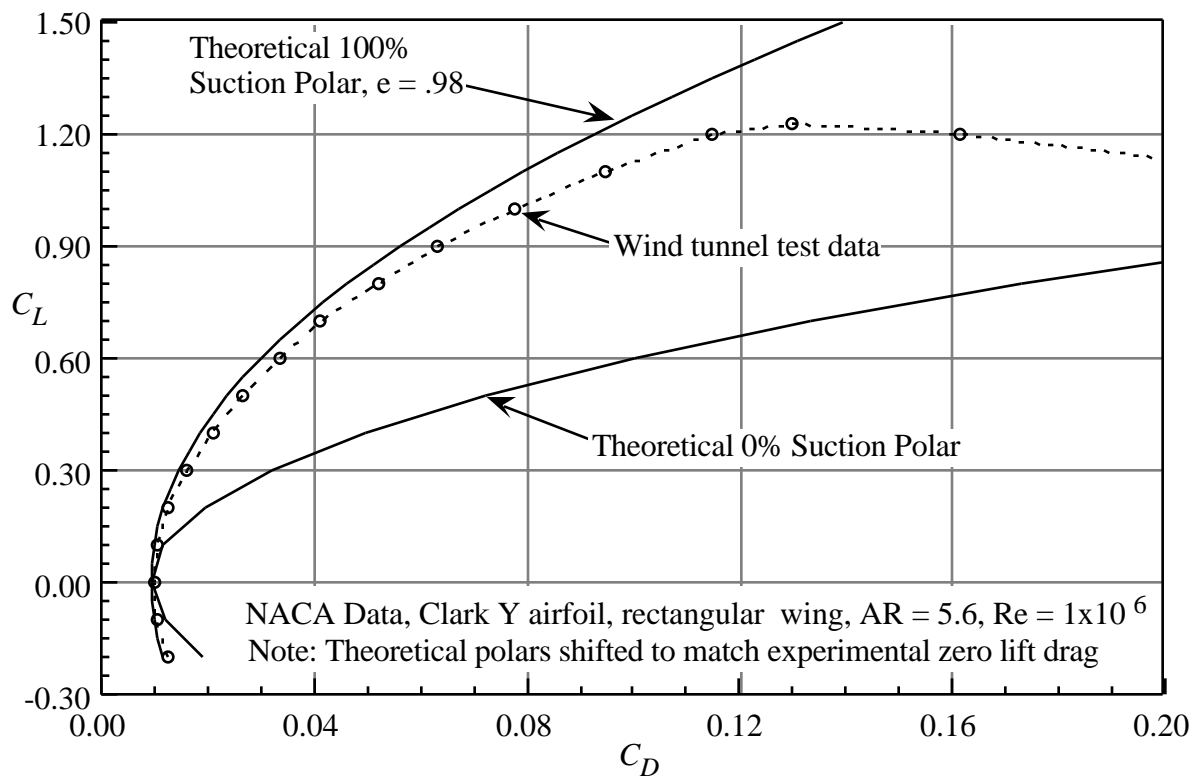


Figure 5-24 Drag performance of simple unswept wing with a Clark-Y airfoil.

It is difficult to identify the initial flow breakdown using the drag polar. Often you can identify flow breakdown more clearly by plotting the axial force as a function of normal force. In this plot the axial force should initially decrease, as described above. When the airfoil section starts to lose leading edge suction the data displays a sharp “break.” Figure 5-25 illustrates this approach to the examination of wing efficiency.

For configurations with very poor aerodynamic efficiency, the 0% suction force provides a good estimate of the vehicle drag. However, 0% suction levels are so inefficient that for most designs this level of performance would be unacceptable and not competitive.

To make estimates of the performance of real configurations, which operate between the two limits, Harry Carlson^{40,41} at NASA Langley established the notion of “attainable” leading edge suction. Based on an extensive analysis of 2D airfoil data, Carlson established an empirical correlation which is used to estimate the fraction of the full suction that should be attained for the specified airfoil, planform and flight condition. Carlson’s concepts are based on linear theory.

Nonlinear effects can be important, and can be exploited. Although the linear theory based concepts described here provide a valuable way of looking at wing designs, nonlinear effects can provide a means of improving performance. Considering nonlinear effects, interactions between thickness and lifting effects can be exploited.⁴²

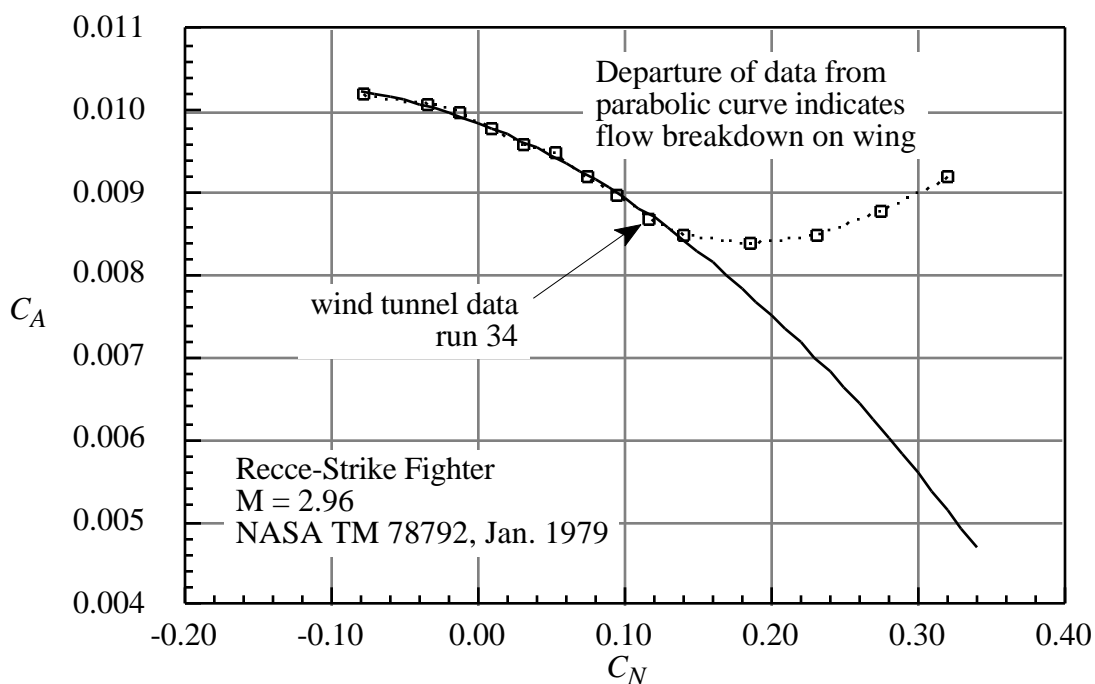
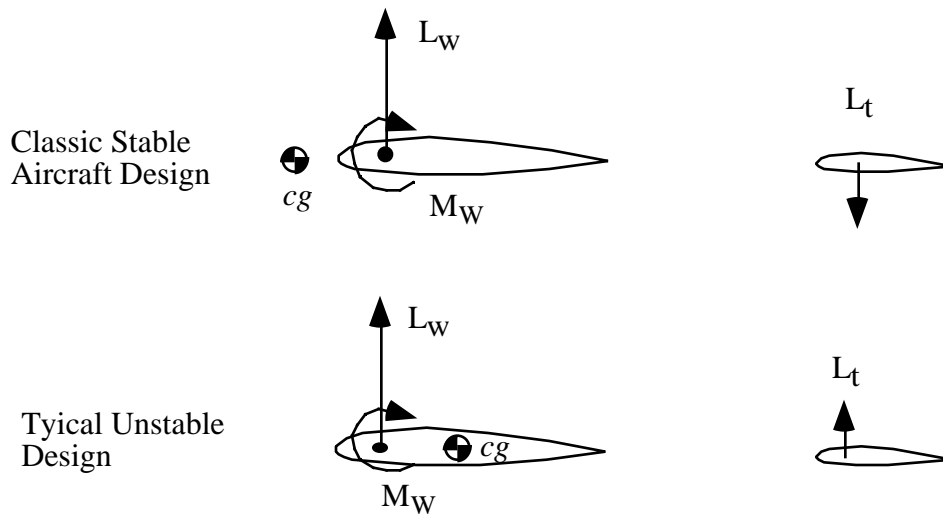


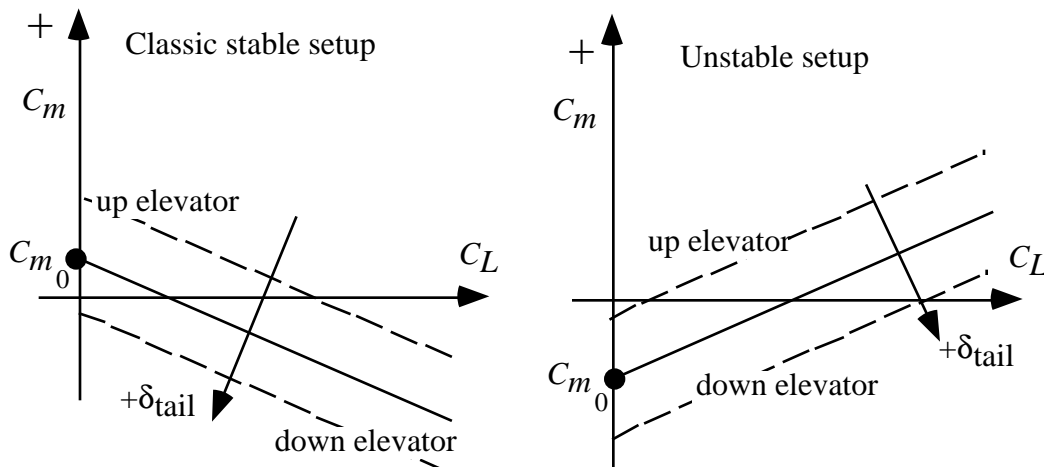
Figure 5-25. Axial force analysis of wing performance.

5.10 Trim Drag

For equilibrium flight the airplane must be trimmed. The forces must be such that the moments about the center of gravity in all axes are zero. To achieve this condition the controls are usually deflected to generate the required trimming moments. Figure 5-26 shows a schematic of the requirement. Two typical situations are shown in Fig. 5-26a. In one case the center of gravity is ahead of the wing center of pressure, the aircraft is stable, and a download on the tail is required to balance the lift of the wing. In the other case the center of gravity is behind the wing center of pressure, the airplane is unstable, and an upload on the tail is required to balance the lift of the wing. Other situations are possible, but these two illustrate the key idea.



a) surface lift requirements for trim



b) idealizations of design requirements

Figure 5-26. Examination of the configuration setup required for trim.

Part *b* of Fig. 5-26 illustrates the difference between stable and unstable configurations. For a stable airplane the basic C_{m0} is typically positive, while for an unstable aircraft the basic C_{m0} is negative. In each case, a control has to be deflected over a range of settings to maintain trim over a range of lift coefficients (unless the configuration is neutrally stable). On modern aircraft the control could be the deflection of the thrust by thrust vectoring.

Control surface deflections change the drag from the reference undeflected value. This difference in drag could be termed a "trim drag." There are many definitions of trim drag. Definitions differ because it is difficult to be precise in defining trim drag. Some definitions contain only the

drag due to the lift of the trimming surface. Some analyses allow for a negative trim drag. However, for a given flight condition the total lift must be fixed, and any change in lift on the trimming surface requires a change in lift, and hence drag, on the primary surface. On a well designed aircraft the trim drag should be small. Canard concepts are often considered advantageous because both the canard and wing supply positive lift to trim, whereas for traditional aft-tail configurations the tail load is negative and the wing must operate at a higher lift to compensate. However, for modern aft-tail designs the tail load is near zero, resulting in little trim drag.

Trim drag has always been an important consideration in airplane design. However, trim drag became especially important with the development of stability and control augmentation systems that allowed the designer much greater freedom in the choice of a center of gravity location. Natural static stability was no longer required. The static stability condition had frequently made it difficult to obtain minimum trim drag. This meant that trim drag could become a key criteria for the placement of the center of gravity in a configuration (this is part of the motivation for so-called control configured vehicle, CCV, concepts).

Trim drag is especially important for several specific classes of aircraft. Supersonic aircraft demand special consideration because of the aerodynamic center shift from subsonic to supersonic flight. To control trim drag as well as stability, fuel is transferred fore and aft between subsonic and supersonic flight to achieve proper balance on supersonic cruise aircraft. Variable sweep wing aircraft also have aerodynamic center locations that vary with wing sweep, potentially leading to high values of trim drag. Finally, maneuvering aircraft can suffer high trim drag at high lift coefficients, severely limiting sustained turn performance. This was especially true of the first generation of supersonic capable fighters. Examples of the contribution of trim drag to the total drag are shown in Figure 5-27, taken from Nicolai.⁴³

A more useful approach to the trim drag analysis is to consider the value of “trimmed drag”. In this approach it is difficult to define a specific trim drag value. The best way to assess the trim penalty is to define the difference between the minimum drag attainable for the system and the minimum trimmed drag for a specified center of gravity position. This provides the designer with a measure of the drag penalty being paid for a particular center of gravity location. This approach also demonstrates directly the connection between static margin and minimum trimmed drag. Different configuration concepts lead to different values of static margin to obtain minimum trimmed lift. In general, for aft swept wings aft tail configurations, the minimum trimmed drag occurs at a slightly unstable center of gravity (5-10%?), canard configurations have minimum trim drag at slightly more unstable conditions (15%?), and forward swept wing canard configurations must be even more unstable to achieve minimum trimmed drag (the X-29 is about 30-35% unstable). Many studies of these fundamental properties of various configuration concepts have been made. See the study by Landfield and Rajkovic⁴⁴ and the references contained therein for more information.

a) C-141 at $M = 0.75$

b) F-111A

Figure 5-27. Contributions to drag for two configurations.⁴³

Several key papers examining trim drag from a nearfield point of view have been written. They are by McKinney and Dollyhigh,³⁸ Lutze,⁴⁵ and Sachs.⁴⁶ In the nearfield, extreme care must be taken to include the downwash incidences and induced angles of attack correctly. Alternately, an analysis can be made in the Trefftz plane. Lamar²⁶ developed a code for finding the minimum trimmed induced drag for two surfaces, and this was extended to include (approximately) the effects of profile drag by Mason.²⁷ Note that a farfield analysis which combines the minimization of induced drag and wave drag due to lift has been presented by Tulinius and Margason.⁴⁷ A more general approach to treat multiple surfaces was given by Kuhlman.⁴⁸ More recently, three surface configuration have been introduced, and the three surface minimum trim drag problem has been solved by Goodrich, Sliwa, and Lallman⁴⁹ using a nearfield approach.

An example of the possible dramatic effects of cg location on trimmed drag is presented in Figure 5-28.²⁷ All the results contained in the figure are for the minimum trimmed drag at different values of a specified cg location. These results were obtained during early forward-swept wing configuration studies, and illustrate why an aft cg position and resulting highly unstable configuration are required to obtain the full benefits of a forward swept wing configuration simi-

lar to the X-29.* The very high drag values reflect a transonic maneuver condition. Trim drag should be much smaller for the cruise condition (certainly less than 2-4%). As shown here, modern technology should allow the aircraft to fly with no trim drag. The difference between the minimum trimmed drag at $\Delta x_{cg} = -40$ and any other cg could be considered the trim drag. The figure contains both induced and profile drag contributions to the total trimmed drag. As the cg moves forward (x positive in this nomenclature, $x = 0$ corresponds to neutral stability), the additional load on the canard leads to a rapidly increasing value of the minimum trimmed drag. Because of the increasing load on the canard, the canard airfoil section becomes important. Near the cg for minimum drag the canard airfoil is not important because the canard is lightly loaded. This figure shows why canard configurations are most efficient when used with unstable configuration concepts. Stable canard configurations are not necessarily the most efficient aerodynamically. Because of the high loads on a stable canard configuration, the canard airfoil section is very carefully selected. Specifically, it is usually highly cambered to achieve the high lift coefficients, and has a small leading edge radius so that it will stall before the main wing.

Figure 5-28 Minimum trimmed drag throughout a range of balance locations, including the effect of canard airfoil section.²⁷

* Note that the hydraulic power used to activate the canard to achieve apparent stability is obtained from the engine, reducing thrust and resulting in increased fuel flow. Thus, in essence, some trim drag benefits are gained at the expense of increased fuel usage to control the unstable vehicle.

5.11 Current Issues for Drag Calculation Using Computational Aerodynamics

Because of the quest for reduced drag, and the difficulty in computing and measuring small changes in drag, numerous disputes have arisen in aerodynamics. Confusion introduced by non-standard drag nomenclature also contributes to these spirited debates. One recent issue was the so-called sheared wing-tip drag reduction controversy. Here it was speculated that wing tip shaping could lead to span e 's greater than one for planar planforms.⁵⁰ This conclusion arose based on both computations and wind tunnel tests. Refined computational investigations,⁵¹ illustrating the need to study computational solution convergence carefully as shown elsewhere in this text, resulted in the conclusion that e 's greater than one were not actually computed. However, it is clear that wing tip planform shaping can lead to improved aerodynamic efficiency.

Another area currently attracting attention is the search for more fundamental understanding of drag. These theories differ significantly from the accepted approach to drag. One key example is due to Yates.⁵²

In addition to the efforts to reduce drag due to lift by tip shaping, use of winglets, tip sails, and canard configurations among others, significant efforts are being made to reduce skin friction drag. They include efforts to obtain laminar flow through passive means (NLF), suction, or a combination known as hybrid natural laminar flow control. Turbulent friction reduction techniques are also being developed. Riblets are perhaps the most well known means. A recent AIAA book reviews this area.⁵³

5.12 Exercises

1. Derive equations 5-7 and 5-8.
2. Derive equations 5-31 and 5-32.
3. Get a copy of **LIDRAG** and check it against the the known values of the span e for an elliptic and a triangular load distribution. How do your results compare?
4. Use experimental results and show quantitatively that Fig. 5-11 is correct.
5. Get a copy of **FRICITION**. Repeat the check case in the user's manual. Then examine the skin friction values in Table 5-1. Are they reasonable?
6. Find the shape of the Karman ogive, the body with minimum wave drag for a given length and base area.

5.13 References

1. Strang, W.J., and McKinlay, R.M., "Concorde in Service," *Aeronautical Journal*, February, 1979.
2. Bavitz, et al., "Configuration Development of Advanced Fighters," Vol. 3, Concept Definition and Validation, AFWAL-TR-3142, November 1980.
3. Sloof, J.W., ed., "Technical Status Review on Drag Prediction and Analysis from Computational Fluid Dynamics: State of the Art," AGARD-AR-256, May 1988.
4. Aerodynamic Drag, AGARD CP-124, 1973.
5. Aircraft excrescence Drag. AGARD 1981.
6. Aircraft Drag Prediction, AGARD-R-723, 1985.
7. Drag Reduction Techniques, AGARD ????
8. Covert, E.E., ed., *Thrust and Drag: Its Prediction and Verification*, AIAA, New York, 1985.
9. Hoerner, S., *Fluid Dynamic Drag*, originally published by the author, and available from Hoerner Fluid Dynamics, 7528 Stauton Place, NW, Albuquerque, NM 87120. (505) 898-0533.
10. Torenbeek, E., *Synthesis of Subsonic Airplane Design*, Delft University Press, Delft, 1982.
11. Whitford, R., *Design for Air Combat*, Jane's London, 1987.
12. Huenecke, K., *Modern Combat Aircraft Design*, Naval Institute Press, Annapolis, 1987.
13. Haines, A.B., "Subsonic Aircraft Drag: An Appreciation of the Standards," *The Aeronautical Journal of the Royal Aeronautical Society*, Mar. 1968, pp. 253-266.
14. Küchemann, D., *The Aerodynamic Design of Aircraft*, Pergamon Press, Oxford, 1978.
15. Lynch, F.T., "Commercial Transports—Aerodynamic Design for Cruise Performance Efficiency," *Transonic Aerodynamics*, Nixon, D., ed., Progress in Astronautics and Aeronautics, Vol. 181, AIAA New York, 1982.
16. Shevell, "Aerodynamic Bugs: Can CFD Spray Them Away?" AIAA Paper 85-4067, Oct. 1985.
17. Rooney, E.C., "Thrust-Drag Accounting Methodology," in *Thrust and Drag: Its Prediction and Verification*, Covert, E.E., ed., AIAA, New York, 1985.
18. Ashley, H., and Landahl, M., *Aerodynamics of Wings and Bodies*, Addison-Wesley, Reading, 1965, sections 1.6, 6.6, 7.3 and 9.2,
19. Heaslet, M.A., and Lomax, H., "Supersonic and Transonic Small Perturbation Theory," in *General Theory of High Speed Aerodynamics*, W.R. Sears, ed., Princeton University Press, 1954 , sec. D,14: pp 221-229.
20. Liepman, H.W., and Roshko, A., *Elements of Gasdynamics*, John Wiley, New York, 1957, pp. 235-239.
21. Harris, R.V., "An Analysis and Correlation of Aircraft Wave Drag," NASA TM X-947, 1964.

5.13 References

22. Sears, W.R., "On Calculation of Induced Drag and Conditions Downstream of a Lifting Wing," *Journal of Aircraft*, Vol. 11, No. 3, March 1974, pp.191-192.
23. Thwaites, B., ed., *Incompressible Aerodynamics*, Oxford, 1960, pp. 454-457, 523-527.
24. Mason, W.H., Mackenzie, D., Stern, M., Ballhaus, W.F., and Frick, J., , "An Automated Procedure for Computing the Three Dimensional Transonic Flow over Wing-Body Combinations, Including Viscous Effects," AFFDL-TR-77-122, Feb. 1978.
25. Milne-Thomson, *Theoretical Aerodynamics*, Dover, New York, pp 218-219
26. Lamar, J.E., "A Vortex Lattice Method for the Mean Camber Shapes of Trimmed Non-Coplanar Planforms with Minimum Vortex Drag," NASA TN D-8090, June, 1976.
27. Mason, W.H., "Wing-Canard Aerodynamics at Transonic Speeds—Fundamental Considerations on Minimum Drag Spanloads," AIAA Paper 82-0097, Jan. 1982.
28. Paterson, J.H., MacWilkenson, D.G., and Blackerby, W.T., "A Survey of Drag Prediction Techniques Applicable to Subsonic and Transonic Aircraft Design," in *Aerodynamic Drag*, AGARD CP 124, April 1973.
29. Jones, R.T. *Wing Theory*, Princeton University Press, Princeton, 1991.
30. Whitcomb, R.T., "A Study of the Zero Lift Drag-Rise Characteristics of Wing-Body Combinations near the Speed of Sound," NACA Report 1273, 1956.
31. Mendenhall, C., *Delta Wings—Convair's High Speed Planes of the Fifties and Sixties*, Motorbooks International, Osceola, WI, 1983.
32. Anon., *Aireviews jet Fighters of the World Part 2*, Kantosha Co. Ltd., Tokyo, 1965 (in Japanese).
33. Stuart, William G., "Northrop F-5 Case Study in Aircraft Design," AIAA Professional Study Series, Sept. 1978.
34. Emlinton, E., and Lord W.T., "Note on the Numerical Evaluation of the Wave Drag of Smooth Slender Bodies Using Optimum Area Distributions for Minimum Wave Drag," *Journal of the Royal Aeronautical Society*, Vol. 60, Jan. 1956, pp. 61-63.
35. Robins, A.W., Dollyhigh, S.M., Beissner, F.L., Jr., Geiselhart, K., Martin, G.L., Shields, E.W., Swanson, E.E., Coen, P.G., Morris, S.J., Jr., "Concept Development of a Mach 3.0 High-Speed Civil Transport," NASA TM 4058
36. Hutchison, M., Unger, E., Mason, W.H., Grossman, B., and Haftka, R., "Variable-Complexity Aerodynamic Optimization of an HSCT Wing Using Structural Wing-Weight Equations," AIAA Paper 92-0212, Jan. 1992.
37. Buckner, J.K., Benepe, D.B., Hill, D.W., "Aerodynamic Design Evolution of the F-16," AIAA Paper 74-935, 1974.
38. McKinney, L.W., and Dollyhigh, S.M., "Some Trim Drag Considerations for Maneuvering Aircraft," *Journal of Aircraft*, Vol. 8, No. 8, Aug. 1971, pp.623-629.
39. Raymer, D.P., *Aircraft Design: A Conceptual Approach*, AIAA, Washington, 1989.
40. Carlson, H.W., Mack, R.J., and Barger, R.L., "Estimation of Attainable Leading Edge Thrust for Wings at Subsonic and Supersonic Speeds," NASA TP 1500, 1979.

5.13 References

41. Mann, M.J., and Carlson, H.W., "An Assessment of Current Methods for Drag-Due-To-Lift Minimization at Supersonic Speeds," AIAA Paper 91-3302, Sept. 1991.
42. Mason, W.H., and DaForno, G., "Opportunities for Supersonic Performance Gains Through Non-Linear Aerodynamics," AIAA Paper 79-1527, July 1979.
43. Nicolai, L.M., *Fundamentals of Aircraft Design*, METS, Xenia, 1975.
44. Landfield, J.P., and Rajkovic, D., "Canard/Tail Comparison for an Advanced Variable-Sweep-Wing Fighter," AIAA Paper 84-2401, October 1984.
45. Lutze, F.H., "Trimmed Drag Considerations," *Journal of Aircraft*, Vol. 14, No. 6, June 1977, pp.544-546.
46. Sachs, G., "Minimum Trimmed Drag and Optimum c.g. Position," *Journal of Aircraft*, Vol. 15, No. 8, Aug. 1978, pp. 456-459.
47. Tulinius, J.R., and Margason, R.J., "Aircraft Aerodynamic Design and Evaluation Methods," AIAA Paper 76-15, Jan. 1976.
48. Kuhlman, J.M., "Higher Order Farfield Drag Minimization for a Subcritical Wing Design," *Journal of Aircraft*, Vol. 17, No. 9, Sept. 1980, pp. 648-655.
49. Goodrich, K.H., Sliwa, S.M., and Lallman, F.J., "A Closed-Form Trim Solution Yielding Minimum Trim Drag for Airplanes with Multiple Longitudinal Control Effectors," NASA TP 2907, May 1989.
50. VanDam, C.P., "Induced-Drag Characteristics of Crescent-Moon-Shaped Wings," *Journal of Aircraft*, Vol. 24, No. 2, Feb. 1987. pp. 115-119.
51. Smith, S.C., and Kroo, I.M., "A Closer Look at the Induced Drag of Crescent-Shaped Wings," AIAA Paper 90-3063, Aug. 1990.
52. Yates, J.E., "Prediction of Drag and Lift: A Viscous/Thermodynamic Approach," A.R.A.P. Report No. 651, Aug. 1990 (presented at an AIAA Short Course, Portland, Oregon, Aug. 23-24, 1990).
53. Bushnell, D.M., and Hefner, J.N., ed., *Viscous Drag Reduction in Boundary Layers*, AIAA Progress in Astronautics and Aeronautics Series, Vol. 123, AIAA, Washington, 1990.